

**Unscented Transform Performance Assessment
of
Adaptive LCMV Filters and Radioaltimeters**

Ronaldo Sebastião Ferreira Júnior

DISSERTAÇÃO DE MESTRADO EM ENGENHARIA ELÉTRICA
DEPARTAMENTO DE ENGENHARIA ELÉTRICA

Brasília, Maio de 2015

**FACULDADE DE TECNOLOGIA
UNIVERSIDADE DE BRASÍLIA**

UNIVERSIDADE DE BRASÍLIA
FACULDADE DE TECNOLOGIA
DEPARTAMENTO DE ENGENHARIA ELÉTRICA

Unscented Transform Performance Assessment
of
Adaptive LCMV Filters and Radioaltimeters

Ronaldo Sebastião Ferreira Júnior

ORIENTADOR: João Paulo Carvalho Lustosa da Costa
COORIENTADOR: Ricardo Zelenovsky

DISSERTAÇÃO DE MESTRADO EM ENGENHARIA
ELÉTRICA

PUBLICAÇÃO: PPGEE.DM - 593/2015
BRASÍLIA/DF: Maio - 2015

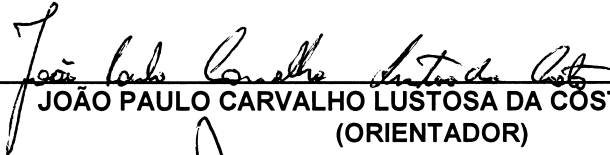
**UNIVERSIDADE DE BRASÍLIA
FACULDADE DE TECNOLOGIA
DEPARTAMENTO DE ENGENHARIA ELÉTRICA**

**UNSCENTED TRANSFORM PERFORMANCE ASSESSMENT OF
ADAPTIVE LCMV FILTERS AND RADIOALTIMETERS**

RONALDO SEBASTIÃO FERREIRA JÚNIOR

DISSERTAÇÃO DE MESTRADO SUBMETIDA AO DEPARTAMENTO DE ENGENHARIA ELÉTRICA DA FACULDADE DE TECNOLOGIA DA UNIVERSIDADE DE BRASÍLIA, COMO PARTE DOS REQUISITOS NECESSÁRIOS PARA A OBTENÇÃO DO GRAU DE MESTRE.

APROVADA POR:



JOÃO PAULO CARVALHO LUSTOSA DA COSTA, Dr., ENE/UNB
(ORIENTADOR)



ADONIRAN JUDSON DE BARROS BRAGA, Dr., ENE/UNB
(EXAMINADOR INTERNO)



JOSÉ ANTÔNIO APOLINÁRIO JUNIOR, Dr., IME
(EXAMINADOR EXTERNO)

Brasília, 15 de maio de 2015.

FICHA CATALOGRÁFICA

FERREIRA JÚNIOR, RONALDO SEBASTIÃO

Unscented Transform Performance Assessment of Adaptive Linearly Constrained Minimum Variance Filters and Radioaltimeters [Distrito Federal] 2015.

ix, 57p., 297 mm (ENE/FT/UnB, Mestre, 2015) Dissertação de Mestrado – Universidade de Brasília. Faculdade de Tecnologia.

1. Arranjos de Antenas
2. Filtros de Posto Reduzido
3. Transformada da Incerteza
4. Processamento de Sinais
5. Filtros Adaptativos

I. ENE/FT/UnB

II. Título (série)

REFERÊNCIA BIBLIOGRÁFICA

FERREIRA JÚNIOR, R. S., (2015). *Unscented Transform Performance Assessment of Adaptive Linearly Constrained Minimum Variance Filters and Radioaltimeters*, Dissertação de Mestrado em Engenharia Elétrica, Publicação PPGEE.DM-593/2015, Departamento de Engenharia Elétrica, Universidade de Brasília, Brasília, DF, 57p.

CESSÃO DE DIREITOS

AUTOR: Ronaldo Sebastião Ferreira Júnior

TÍTULO: *Unscented Transform Performance Assessment of Adaptive Linearly Constrained Minimum Variance Filters and Radioaltimeters*

GRAU: Mestre

ANO: 2015

É concedida à Universidade de Brasília permissão para reproduzir cópias desta dissertação de mestrado e para emprestar ou vender tais cópias somente para propósitos acadêmicos e científicos. O autor reserva outros direitos de publicação e nenhuma parte dessa dissertação de mestrado pode ser reproduzida sem autorização por escrito do autor.

Ronaldo Sebastião Ferreira Júnior

CAVP - Rua 08 - Ch. 218 - Casa 09

72.110-800 Brasília – DF – Brasil.

Dedicatória

Aos meus pais:

Ronaldo Sebastião e Susy, que possibilitaram todas as minhas conquistas devido ao seu sacrifício e amor.

Ao meu irmão:

Diogo, meu grande amigo, que me apoiou em todas as horas.

Aos meus avós e tio:

Yoshio, Yochie e Tony, que a quem devo grande parte de tudo que eu aprendi e me inspirei na vida.

Ronaldo Sebastião Ferreira Júnior

Agradecimentos

A Deus por me guiar e confortar durante toda as horas da minha vida.

Muito devo ao meu orientador Professor João Paulo Carvalho Lustosa da Costa, por sua excelente tutela, por todo apoio, confiança e paciência, por todas as enormes oportunidades de crescimento acadêmico, incentivos e respeito, ter me tratado como amigo em horas apropriadas e como aluno em horas de profissionalismo. Devo dizer que é um prazer trabalhar ao seu lado e espero continuar o laço de amizade e profissional por um longo tempo.

Um agradecimento especial ao meu coorientador, Professor Ricardo Zelenovsky, a quem admiro e me inspirou a perseguir a carreira acadêmica, durante todo o tempo da graduação, com suas excelentes aulas.

Ao colega Marco Antônio Marques Marinho, uma pessoa brilhante, a quem sempre pude contar com sua ajuda e prestatividade.

Aos membros da secretaria do ENE, em especial a Ana Carolina por sua disponibilidade, prestatividade e incrível capacidade incrível de resolver problemas burocráticos à qualquer hora. Sem vocês provavelmente não conseguiria o título de mestre.

Por todas as pessoas que passaram por minha vida, possibilitando meu crescimento como pessoa humana, me ensinaram e mostraram tudo que mantém o brio e viço do meu viver.

Ronaldo Sebastião Ferreira Júnior

Avaliação da Performance da Transformada da Incerteza em Filtros Adaptativos de Mínima Variância e Radioaltímetros

Autor: Ronaldo Sebastião Ferreira Júnior

Orientador: João Paulo Carvalho Lustosa da Costa

Coorientador: Ricardo Zelenovsky

Programa de Pós-graduação em Engenharia Elétrica

Brasília, Maio de 2015

Nas últimas décadas técnicas em arranjos de antenas, filtragem adaptativa e processamento de sinais têm recebido grande atenção, por sua versatilidade, possibilidade de aplicação em sistemas embarcados, RADARes, SONARes e afins. Várias técnicas de filtragem adaptativa e *beamforming* têm sido desenvolvidas desde a década de 1960. Desde então, a complexidade de diversos sistemas e modelos estocásticos vem crescendo de uma forma exponencial, para isto é necessário a adoção de novas técnicas de simulação como a Transformada da Incerteza, de modo que as tradicionais técnicas de simulação como a de Monte Carlo sejam auxiliadas ou substituídas, a fim de obter celeridade no lançamentos de novos produtos e tecnologias no mercado.

A filtragem de posto reduzido possibilita a maximização e a otimização da performance da adaptação de filtros adaptativos, além de reduzir a redundância dos sinais recebidos, por meio da redução da dimensão do sinal recebido do arranjo de antenas, com isto, facilita-se o armazenamento de sinais recebidos para pós-processamento e afins.

Este trabalho tem como foco a verificação e estudo da performance da Transformada da Incerteza para a simulação de filtros de posto reduzido e radioaltímetros.

Palavras Chave: Arranjos de Antenas, Posto Reduzido, Filtros de Mínima Variância, Transformada da Incerteza, UT, Radioaltímetro.

Unscented Transform Performance Assessment of Adaptive LCMV Filters and Radioaltimeters

Author: Ronaldo Sebastião Ferreira Júnior

Supervisor: João Paulo Carvalho Lustosa da Costa

Co-supervisor: Ricardo Zelenovsky

Programa de Pós-graduação em Engenharia Elétrica

Brasília, May of 2015

In the last decades, antenna arrays techniques, adaptive filtering and signal processing have been in great focus due to its versatility, embedded systems applications, RADARs, SONARs, etc. Various adaptive filtering and beamforming techniques have been developed since the 1960's, and along with those, the performance assessment complexity of stochastic systems simulations has been increasing in a exponential rate. It is mandatory to adopt and develop new simulational techniques, like the Unscented Transform, in order to aid or replace the traditional Monte Carlo simulation, in order to give celerity to the development time of new products and technologies for the market.

The reduced rank filtering allows a faster adaptation time for adaptive filters and the elimination of redundant information of an antenna array, optimizing the raw storage for post processing and treatment.

The focus of this work is to evaluate the Unscented Transform performance assessment over reduced rank filters and radioaltimeters.

Keywords: Antenna Arrays, Reduced Rank, Linearly Constrained Minimum Variance Filters, Unscented Transform, Radioaltimeter.

CONTENTS

1	SUMÁRIO	1
2	INTRODUCTION	8
3	DATA MODEL	15
3.1	NOTATION	15
3.2	KRONECKER OPERATORS	15
3.2.1	KRONECKER PRODUCT	16
3.2.2	KRONECKER SUM	16
3.2.3	KRONECKER SUM OF VECTORS	16
3.3	UNSCENTED TRANSFORM	17
3.4	PHASE SHIFT KEYING MODULATION	18
3.4.1	BINARY PSK MODULATION	18
3.5	DATA MODEL FOR LCMV FILTERS	19
3.6	NON-ADAPTIVE LCMV FILTERS	21
3.7	LCMV-LMS ADAPTIVE FILTERS	22
3.8	REDUCED RANK LCMV-LMS ADAPTIVE FILTERS	23
4	UNSCENTED TRANSFORM	25
4.1	GENERALIZATION OF STOCHASTIC MODELS AND MONTE CARLO SIMULATIONS	25
4.2	UNSCENTED TRANSFORM PRELUDE	26
4.3	COMPUTATION OF THE UT	27
4.3.1	FINDING THE STATISTICAL MOMENTS OF AN UNKNOWN PDF WITH THE TAYLOR-MACLAURIN EXPANSION	27
4.3.2	CHOOSING THE SIGMA POINTS AND COMPUTING THE WEIGHT POINTS	28
4.3.3	COMPUTATION OF THE UT FOR THE UNITARY VARIANCE, ZERO-MEAN, GAUSSIAN DISTRIBUTION	30
4.4	UT CONVERGENCE VS MONTE CARLO CONVERGENCE	33
4.5	APPLYING THE UT FOR SIMULATIONS	34
4.6	NUMERICAL SIMULATIONS	37
4.6.1	FIRST APPROACH	37
4.6.2	FULL-RANK LCMV SIMULATIONS	38
4.6.3	REDUCED-RANK LCMV SIMULATIONS	39

4.6.4	REDUCED-RANK VS FULL-RANK LCMV FILTERS	41
5	RADIOALTIMETERS	43
5.1	OPERATIONAL PRINCIPLE OF THE RADIOALTIMETER	43
5.1.1	MATHEMATICAL WORKING PRINCIPLE OF THE RADIOALTIMETER.....	44
5.2	PROPOSED DIGITAL RADIOALTIMETER.....	46
5.3	SIMULATION SCENARIO SETUP	48
5.3.1	SIMULATION RESULTS	50
6	CONCLUSION	53
	REFERENCES	54

LIST OF FIGURES

1.1	Função de Probabilidade Gaussiana contínua, em azul, e a discretizada, em verde [1, 2].	2
1.2	Esquema de arranjo de antenas em um filtro LCMV [3, 4].	3
1.4	Esquema do funcionamento do algoritmo LMS [3].	4
1.3	Esquema de um filtro LCMV de posto reduzido com adaptação LMS [5, 3, 6, 7, 8, 9].	4
1.5	Diagrama da abordagem proposta.	5
1.6	Diagrama simplificado do radioaltímetro proposto.	6
2.1	The continuous Gaussian Probability Density Function, in blue, and its four-point discretized Unscented Transform counterpart, in green [1, 2].	9
2.2	Adaptive LCMV filter with its antenna array [3, 4].	10
2.3	Adaptive reduced rank LCMV filter block [5, 3, 6, 7, 8, 9].	10
2.4	Simplified LMS adapting algorithm block [3].	11
2.5	Proposed approach chart.	12
2.6	Simplified diagram of the proposed radioaltimeter.	13
3.1	BPSK constellation.	19
3.2	Simplified block of an ULA and LCMV filter [6, 3].	19
3.3	LCMV adaptive filter [3, 4].	22
3.4	Diagram block of a reduced rank LCMV adaptive filter [5, 3, 6, 7, 9, 8].	24
4.1	3-point UT vs Gaussian PDF.	32
4.2	4-point UT vs Gaussian PDF.	33
4.3	Convergence of Monte Carlo and the UT expectancies.	34
4.4	Convergence of Monte Carlo and the UT variances.	34
4.5	SINR (dB) vs sample numbers, before using 4.34 to calculate the final expectancy for UT curves.	38
4.6	SINR (dB) vs sample numbers, 32 Monte Carlo runs, and 32 UT runs.	38
4.7	SINR (dB) vs sample numbers, 1000 Monte Carlo runs, and 32 UT runs.	39
4.8	Gain (dB) vs DOAs, 1000 Monte Carlo runs and 32 UT runs.	39
4.9	SINR (dB) vs sample numbers, 32 Monte Carlo runs, and 32 UT runs.	40
4.10	SINR (dB) vs sample numbers, 1000 Monte Carlo runs, and 32 UT runs.	40
4.11	Gain (dB) vs DOAs, 1000 Monte Carlo runs and 32 UT runs.	41

4.12	SINR (dB) vs sample numbers, for the reduced-rank and full-rank filters, using the UT.	41
4.13	SINR (dB) vs sample numbers, for the reduced-rank and full-rank filters, using 1000 MC runs.	42
4.14	All beamformers overlapped.	42
5.1	Working diagram of a traditional radioaltimeter [10, 11].	44
5.2	Modulating triangle waveform and its phase delayed version. At the positive or negative voltage peaks, the VCO outputs the center frequency, f_c , summed to the positive or negative Δf peak deviations [10].	45
5.3	Simplified diagram of the proposed radioaltimeter.	49
5.4	Proposed simulation scenario.	50
5.5	Radioaltimeter receiving lobes, before the beamforming.	50
5.6	Voltage output vs altitude for various ADC resolutions.	51
5.7	Voltage output vs altitude for various ADC sampling rates.	51
5.8	Bit-error-rate (BER) for various SNRs, and for the full-rank and reduced rank LCMV-BPSK-Radars	52
5.9	Voltage output vs altitude.	52

LIST OF TABLES

4.1	Zero-mean, Gaussian PDF statistical moments [12, 13, 14].....	30
4.2	Calculated UT Sigma and weight points for the Gaussian noise ($\Phi_{\mathbf{N}}, \Psi_{\mathbf{N}}$) and the BPSK signal ($\Phi_{\mathbf{S}}, \Psi_{\mathbf{S}}$)	36
4.3	Combination of the UT weight points, for each ζ -th iteration.	37

LIST OF SYMBOLS

\otimes	Kronecker product
\oplus	Kronecker sum
$p(\cdot)$	Probability
$(\cdot)^*$	Complex conjugate
$(\cdot)^T$	Transpose of a matrix
$(\cdot)^H$	Complex conjugate transpose of a matrix
j	Complex unity
R_{XX}	Autocorrelation of \mathbf{X}
R_{XY}	Cross-correlation of \mathbf{X} and \mathbf{Y}
$\mathbf{E}[\cdot]$	Expected value

LIST OF ABBREVIATIONS

ADC	Analog-to-Digital Converter
AWGN	Additive White Gaussian Noise
BPSK	Binary Phase Shift Keying
DOA	Direction-of-Arrival
FM	Frequency Modulation
FM-CW	Continuous Wave Frequency Modulation
IF	Intermediate Frequency
INR	Interference-to-noise Ratio
INT	Interfering Signal
LCMV	Linearly Constrained Minimum Variance
LOS	Line-of-Sight
LMS	Least Mean Squares
LPF	Low-pass Filter
Mbps	Megabit per second
MC	Monte Carlo
NLOS	Non-Line-of-Sight
PDF	Probability Distribution Function
PSK	Phase Shift Keying
RR	Reduced Rank
RV	Random Variable
RX	Receiver / Received
SNR	Signal-to-noise Ratio
SINR	Signal-to-noise plus Interference Ratio
SOI	Signal of Interest
TX	Transmitter / Transmitted
UAV	Unmanned Aerial Vehicle
ULA	Uniform Linear Array
UT	Unscented Transform
VCO	Voltage-Controlled Oscillator

Capítulo 1

Sumário

Nas últimas décadas, técnicas em arranjos de antenas, filtragem adaptativa e processamento de sinais têm recebido grande atenção, por sua versatilidade, possibilidade de aplicação em sistemas embarcados, RADARes, SONARes e afins. Várias técnicas de filtragem adaptativa e *beamforming* têm sido desenvolvidas desde a década de 1960. Desde então, a complexidade de diversos sistemas e modelos estocásticos vem crescendo de uma forma exponencial, para isto é necessário a adoção de novas técnicas de simulação como a Transformada da Incerteza, de modo que as tradicionais técnicas de simulação como a de Monte Carlo sejam auxiliadas ou substituídas, a fim de obter celeridade no lançamentos de novos produtos e tecnologias no mercado.

A filtragem de posto reduzido possibilita a maximização e a otimização da performance da adaptação de filtros adaptativos, além de reduzir a redundância dos sinais recebidos, por meio da redução da dimensão do sinal recebido do arranjo de antenas, com isto, facilita-se o armazenamento de sinais recebidos para pós-processamento e afins.

Este trabalho é dividido em seis capítulos: este capítulo sumarizando o trabalho, o Capítulo 2 que trata da introdução do trabalho na língua inglesa, o Capítulo 3 que traz os conceitos matemáticos, modelos de dados para o filtro linear de mínima variância com restrições (LCMV) de complexidade máxima e reduzida (*reduced rank*), o Capítulo 4 que traz a abordagem matemática mais completa da Transformada da Incerteza e suas simulações com filtros LCMV, o Capítulo 5 que traz uma explicação matemática completa de um radioaltímetro convencional, ilustra e simula o radioaltímetro proposto neste trabalho e, finalmente as conclusões estão no Capítulo 6.

Transformada da Incerteza

A Transformada da Incerteza (UT), apresentada no Capítulo 4, permite uma maior celeridade de simulações computacionais de sistemas estocásticos, pela discretização e quantização de funções de distribuição de probabilidade por uma expansão de Taylor [15], criando-se um conjunto de pontos finitos e mensuráveis, com os mesmos momentos estatísticos da função de probabilidade original [2, 1, 16, 17]. Com isso, reduz-se a quantidade efetiva de iterações necessária para a simulação, diferente de uma simulação Monte Carlo, a qual necessita do maior número possível de

iterações para se atingir a convergência dentro de um intervalo de confiança desejável [18, 13, 12].

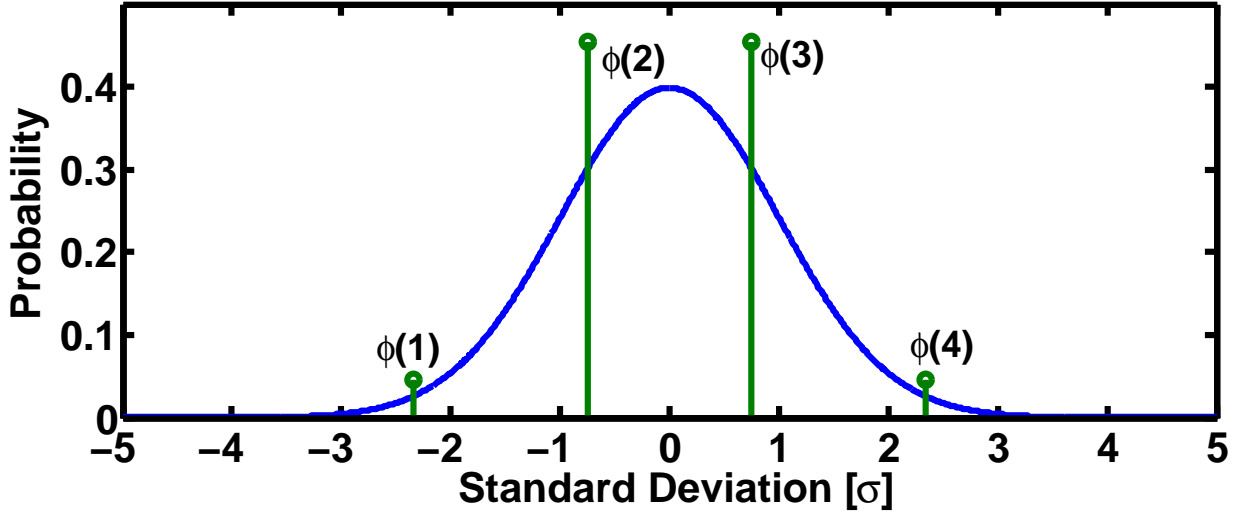


Figure 1.1: Função de Probabilidade Gaussiana contínua, em azul, e a discretizada, em verde [1, 2].

A Figura 1.1 ilustra a função de probabilidade Normal contínua, em azul, e a sua versão discretizada pela Transformada da Incerteza, com quatro pontos, representados pelas variáveis ϕ .

Filtro Linear de Mínima Variância com Restrições

O Filtro Linear de Mínima Variância com Restrições (LCMV - *Linearly Constrained Minimum Variance Filter*), descrito no Capítulo 3, é um *beamformer* que possibilita a conformação do lóbulo de recepção do arranjo de antenas. Supõe-se que a direção de chegada do sinal desejado é conhecida, portanto, uma restrição de fase é imposta ao filtro a fim de se dar maior ganho ao sinal oriundo desta direção; com isso é possível realizar a filtragem espacial dos sinais que chegam ao arranjo de antenas [3, 6, 19]. Como qualquer outro filtro digital, é possível a realização de um filtro LCMV adaptativo, através de diversos algoritmos de adaptação. No escopo deste trabalho é utilizado o algoritmo de Mínimo Erro Quadrático (LMS - *Least Mean Squares*), que minimiza o erro através do cálculo do gradiente estocástico [3, 6].

A Figura 1.2 traz um diagrama simplificado do filtro LCMV adaptativo, o arranjo de antenas é acometido por vários sinais, dos quais um é o sinal de interesse de direção θ_0 , os sinais recebidos formam um vetor $\tilde{\mathbf{x}}$ que é restringido pela matriz de restrição \mathbf{C} , formando o sinal restringido $\tilde{\mathbf{x}}_{\mathbf{c}}$, que é filtrado posteriormente por uma matriz de pesos \mathbf{W} . A matriz de pesos sofre constantes alterações pelo algoritmo adaptativo, a fim de adequar o ganho do filtro de acordo com as condições de recebimento do sinal, como a razão sinal-ruído, a razão sinal-interferidores, entre outras.

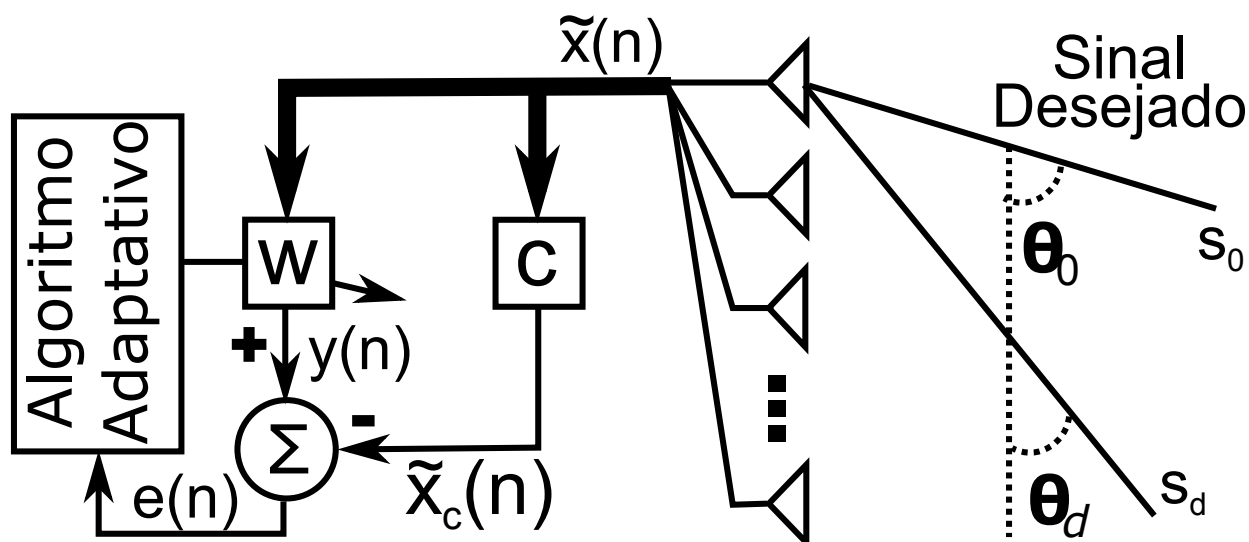


Figura 1.2: Esquema de arranjo de antenas em um filtro LCMV [3, 4].

Filtro de Posto Reduzido

O filtro de Posto Reduzido, descrito no Capítulo 3, é um estágio a mais em um filtro digital adaptativo, que visa reduzir a redundância dos sinais oriundos do arranjo de antenas [6, 7]. Como é realizada uma dupla filtragem, a convergência é atingida mais rapidamente e, com a redução da redundância, facilita-se o armazenamento bruto do sinal para fins de pós-processamento e tratamentos finais.

O filtro de LCMV de Posto Reduzido é ilustrado pela Figura 1.3, onde o sinal restringido sofre uma redução de posto por uma matriz de transformação \mathbf{T} . Após a redução de posto, o sinal é filtrado por um filtro adaptativo de posto reduzido, com os pesos representados por $\bar{\mathbf{W}}$. O algoritmo adaptativo controla os passos de adaptação tanto a matriz de transformação como a do próprio filtro adaptativo, com isso é realizada uma dupla filtragem adaptativa onde a convergência ocorre de maneira mais rápida.

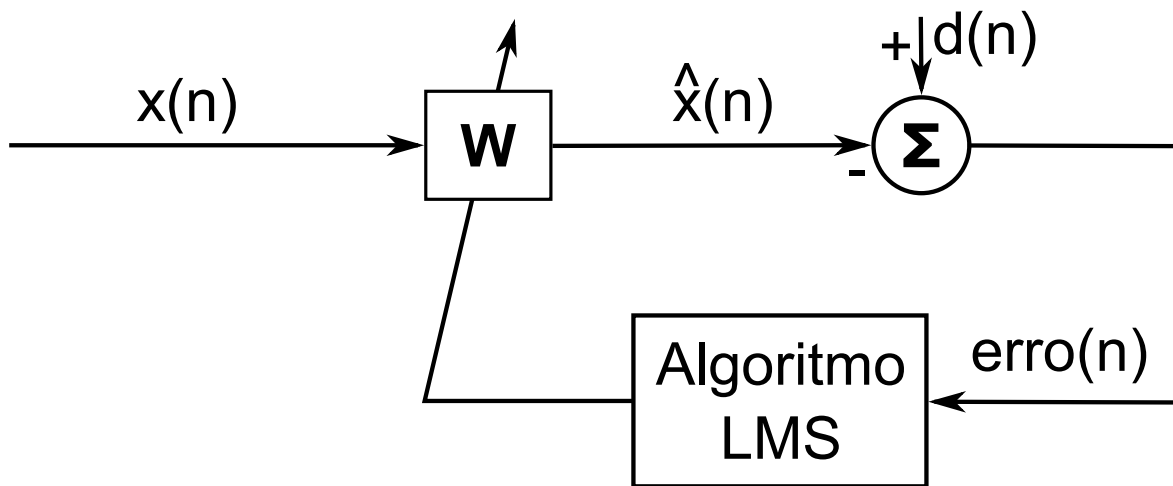


Figura 1.4: Esquema do funcionamento do algoritmo LMS [3].

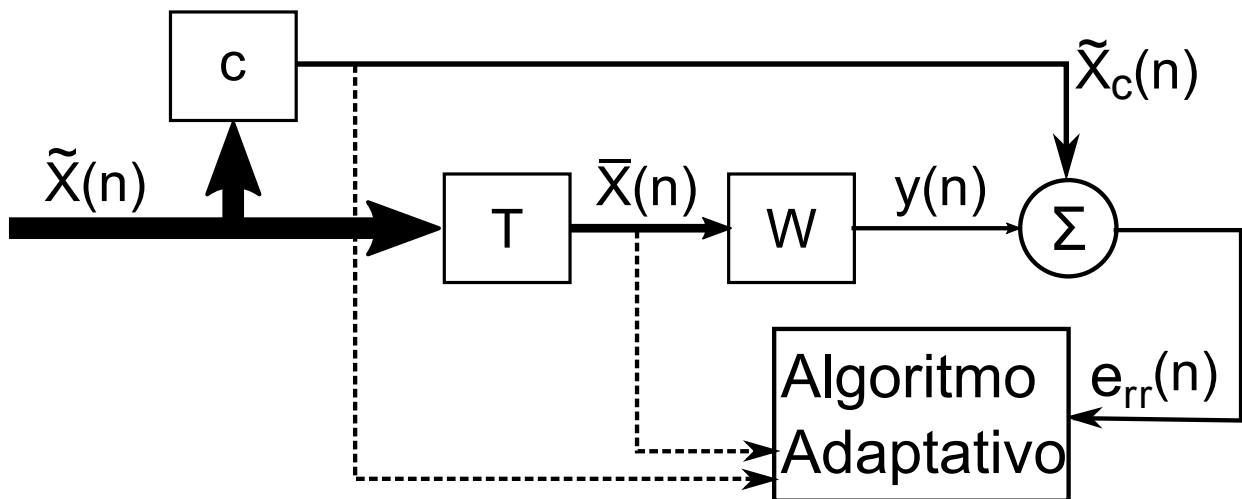


Figure 1.3: Esquema de um filtro LCMV de posto reduzido com adaptação LMS [5, 3, 6, 7, 8, 9].

Algoritmo adaptativo LMS

O algoritmo de Mínimos Erros Quadráticos (*Least Mean Squares* - LMS), apresentado no Capítulo 3, idealizado por Widrow e Hoff na década de 1960, é um importante e muito utilizado algoritmo para filtros adaptativos devido a sua simplicidade e baixo custo computacional [3, 19, 6]. O mesmo se diferencia do algoritmo conhecido por *Steepest Descent* por utilizar uma função de custo baseada no gradiente estocástico do erro, ao invés de uma solução baseada em valores determinísticos nas saídas de um filtro de *Wiener* [6, 19, 3].

A Figura 1.4 mostra a diagramação simplificada do funcionamento do algoritmo LMS, onde seu funcionamento se divide em duas etapas:

1. Calcular o erro estocástico da saída das tomadas de um filtro digital e o sinal desejado;

- Utilizar o erro para realizar o cálculo do gradiente estocástico para se ajustar os pesos das tomadas do filtro digital.

Técnica de simulação proposta com a Transformada da Incerteza

Neste trabalho é proposta uma abordagem que se verifica a performance e confiabilidade da Transformada da Incerteza para filtros adaptativos LCMV, comparando-se com os resultados obtidos de simulações Monte Carlo. A abordagem proposta pode ser resumida em nove passos como mostra a Figura 1.5.

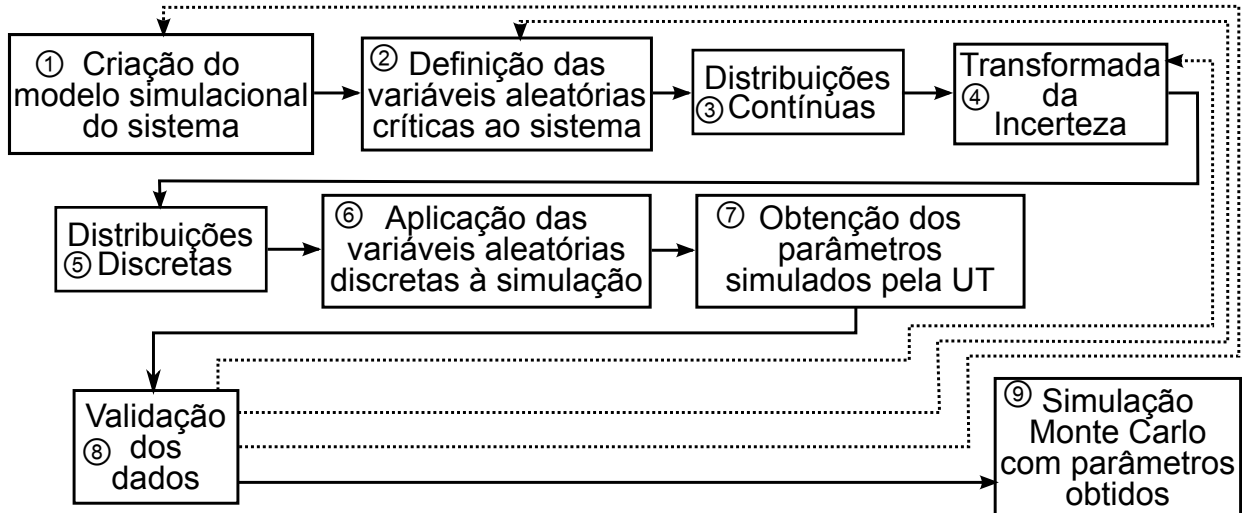


Figura 1.5: Diagrama da abordagem proposta.

São as seguintes as características fundamentais definidas na técnica de simulação proposta aqui tratada:

- Em ①, cria-se o modelo do cenário simulacional, prevendo-se o tipo de ruído e sua variância, modulação, variância e direção de chegada dos sinais desejados e interferentes .
- Em ②, a definição das variáveis aleatórias do sistema é crítica para o correto cômputo da Transformada da Incerteza. Neste trabalho define-se por variáveis aleatórias críticas os parâmetros aleatórios que têm grande impacto sobre o sinal desejado, ou seja, o ruído e interferidores de variância muito superiores aos do sinal desejado.
- Em ③ e ④ aplica-se a Transformada da Incerteza em todas as funções de distribuição de probabilidade contínuas, a fim de se obter um conjunto finito e quantizável de pontos.
- Em ⑤ e ⑥, realiza-se o calculo combinatório de todas as probabilidades envolvidas no sistema, através dos pontos de peso fornecidos pela Transformada da Incerteza.
- Em ⑦, obtém-se o resultado da simulação pela Transformada da Incerteza.

- Por último, em ⑧ e ⑨, verifica-se a validade da simulação pela Transformada da Incerteza através de uma simulação Monte Carlo, comparando-se os resultados e considerando os possíveis erros auferidos ao se discretizar variáveis aleatórias contínuas.

Radioaltímetro proposto

Neste trabalho um novo modelo de radioaltímetro é apresentado. O mesmo faz o uso de filtragem LCMV e de um esquema de modulação BPSK para modelar o lóbulo de recepção, a fim de separar os vários sinais que chegam ao sistema aeromotor para a correta estimação da altura do mesmo.

A Figura 1.6 mostra o diagrama simplificado do radioaltímetro. O radioaltímetro é composto por um radiotransmissor e um radioreceptor de arranjo de antenas. O sinal transmitido é uma onda triangular, que é digitalizada por um conversor análogo digital e modulado por um modulador digital de fase. O sinal recebido pelo arranjo de antenas é demodulado e sofre uma filtragem LCMV, a fim de realizar o modelamento do lóbulo de recepção do arranjo de antenas. O sinal filtrado passa por um processador digital de sinais que detecta o atraso de fase entre o sinal transmitido e o sinal recebido, para calcular a altitude do sistema aeromotor.

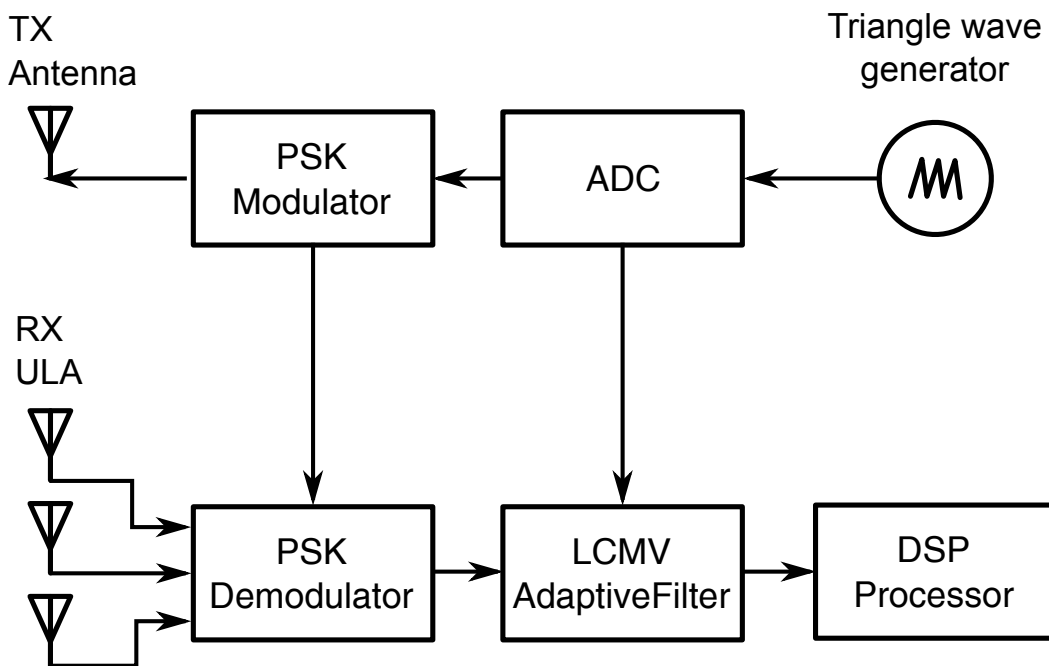


Figura 1.6: Diagrama simplificado do radioaltímetro proposto.

Aplicações

A utilização da Transformada da Incerteza agiliza simulações de sistemas estocásticos, por discretizar as variáveis aleatórias contínuas, implicando-se em ganho acadêmico e econômico, ao se possibilitar o lançamento mais rápido de novas tecnologias e produtos no mercado.

Já os filtros de posto reduzido, por serem filtros versáteis e, pela adição da etapa de redução de posto, possibilitam a convergência mais rápida dos filtros adaptativos. Além de oferecerem a diminuição da redundância dos sinais filtrados, com uma perda mínima, diminuindo-se o custo de armazenamento de sinais brutos para pós-processamento.

No escopo deste trabalho foi desenvolvido um radioaltímetro digital, que utiliza filtros LCMV para a correta estimação da altura de vôo de um sistema embarcado aeromotor.

Validação

Para validar a técnica proposta, um conjunto de simulações numéricas é apresentado na Seção 4.6. O desempenho dos filtros LCMV de posto reduzido é comparado aos filtros LCMV de posto cheio através de técnicas e resultados propostos em [4, 7, 20]. Já a eficácia da Transformada da Incerteza utiliza-se de técnicas propostas e resultados já conhecidos e obtidos em [2, 21, 22, 23, 16].

Já o radioaltímetro proposto e suas simulações são apresentados no Capítulo 5.

Contribuições

Este trabalho apresenta como principal contribuições a validação da Transformada da Incerteza para simulação de sistemas estocásticos, possibilitando simulações mais rápidas ou, no mínimo, uma boa estimativa de parâmetros para simulações Monte Carlo, também apresenta um novo sistema de radioaltímetro digital, que permite a separação dos sinais que chegam ao mesmo, além de tratar acerca da performance dos filtros de posto reduzido em comparação com os de posto cheio.

A validação da Transformada da Incerteza tem grande importância de cunho acadêmico e comercial e os filtros de posto reduzido têm uma grande aplicação prática, desde sistemas de comunicação em massa até aquisição de dados brutos nas mais variadas áreas de engenharia, geologia e economia.

Agradecimentos

O autor gostaria de agradecer o projeto PVE, relacionado a comunicações e navegação via satélite, financiado pela CAPES e pelo CNPq, sob o número de processo 88881.030392/2013-01.

Chapter 2

Introduction

Over the last few decades, antenna arrays techniques, adaptive filtering and signal processing have been in great focus due to its versatility, use embedded systems, RADARs, SONARs, etc. Several adaptive filtering and beamforming techniques have been developed since the 1960's, resulting in an exponential increase of the complexity of those systems, necessitating that improved techniques are required not only for academic purposes but also for commercial and industrial fields where time to market is a critical factor in the success of a product. To overcome these issues, new simulation techniques, such as the Unscented Transform, are essential, in order to give a good setup point to the well known Monte Carlo simulations, raising the celerity of the development and launching of new products and technologies to the market.

The reduced rank filtering allows the maximization and optimization of the adapting filters performance, by reducing the received signal rank, the redundancy and the raw storage needs for post processing of a received antenna array signal are significantly reduced.

This work is divided into six chapters: Chapter 1, which summarizes this work in Brazilian Portuguese, this Chapter 2, the introduction itself, Chapter 3 describing the mathematical concepts, data models for full-rank and reduced rank LCMV adaptive filters and a brief introduction to the Unscented Transform, Chapter 4 brings a detailed mathematical approach for the Unscented Transform and its simulations with LCMV adaptive filters, Chapter 5 illustrating and explaining a conventional analog radioaltimeter and the proposed radioaltimeter, with its simulations. Finally the conclusions are drawn in Chapter 6.

The Unscented Transform

The Unscented Transform (UT), presented in Chapter 4, allows a greater simulation celerity of stochastic systems, by discretizing the continuous random variables with a Taylor expansion [15], creating a finite and quantizable set of points, with the same, or very close, statistical moments of the original random variable [2, 1, 16, 17] and improving the simulation time with a great decrease in the number of iteration steps needed to achieve the convergence within the same, or close, confidence interval a Monte Carlo simulation would achieve with a huge number of iterations

[18, 13, 12].

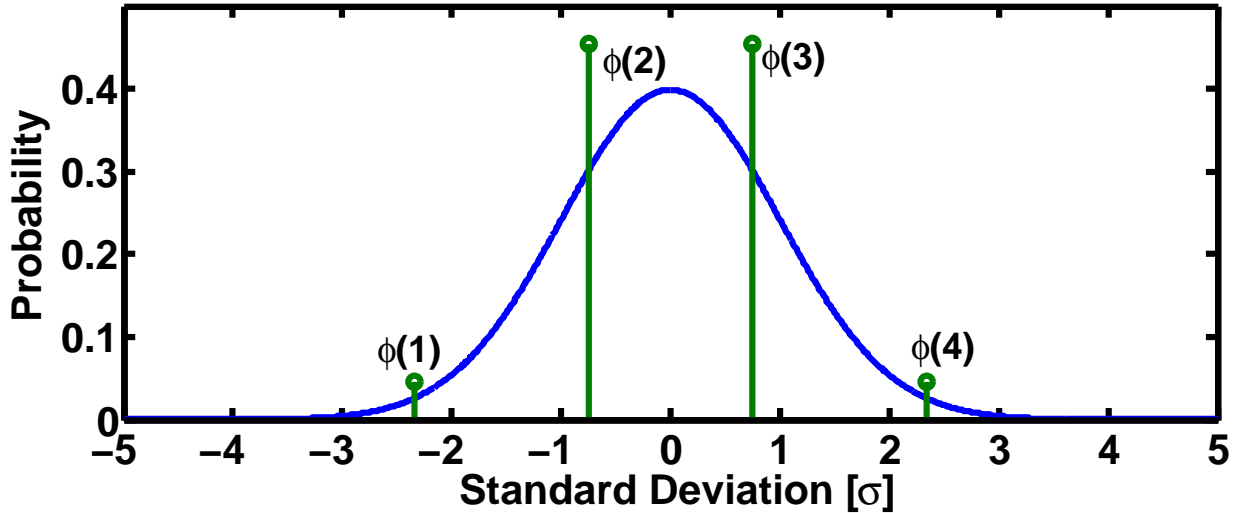


Figure 2.1: The continuous Gaussian Probability Density Function, in blue, and its four-point discretized Unscented Transform counterpart, in green [1, 2].

Figure 2.1 illustrates the Normal Gaussian distribution in blue and its four-point UT discretized counterpart in green.

Linearly Constrained Minimum Variance Filter

The Linearly Constrained Minimum Variance Filter (LCMV), described in Chapter 3, is a beamforming filter which allows the receiving lobe of an antenna array to be modeled electronically. The signal direction of arrival (DOA) is presumed to be known, so a constraint is set to the filter in order to raise the gain of filter at the DOA. Therefore, it is possible to spatially filter the signals impinging on the antenna array [3, 6, 19]. As with any other digital filter, the adaptive LCMV filter is feasible with several adaptive algorithms. In this work the Least Mean Squares (LMS) algorithm is used [3, 6].

Figure 2.2 illustrates a simplified block diagram of the adaptive LCMV filter, where the antenna array is impinged by several signals, in which the one with θ_0 DOA is the signal of interest. The received signals forms the vector $\tilde{\mathbf{x}}$, which is constrained afterwards by the constraint matrix, \mathbf{C} , comprising the constrained signal, $\tilde{\mathbf{x}}_{\mathbf{c}}$. The constrained signal is filtered by a weight matrix, \mathbf{W} , that is continuously adapted by the adaptive algorithm according to the receiving conditions such as the signal-to-noise ratio and the signal-to-interference ratio.

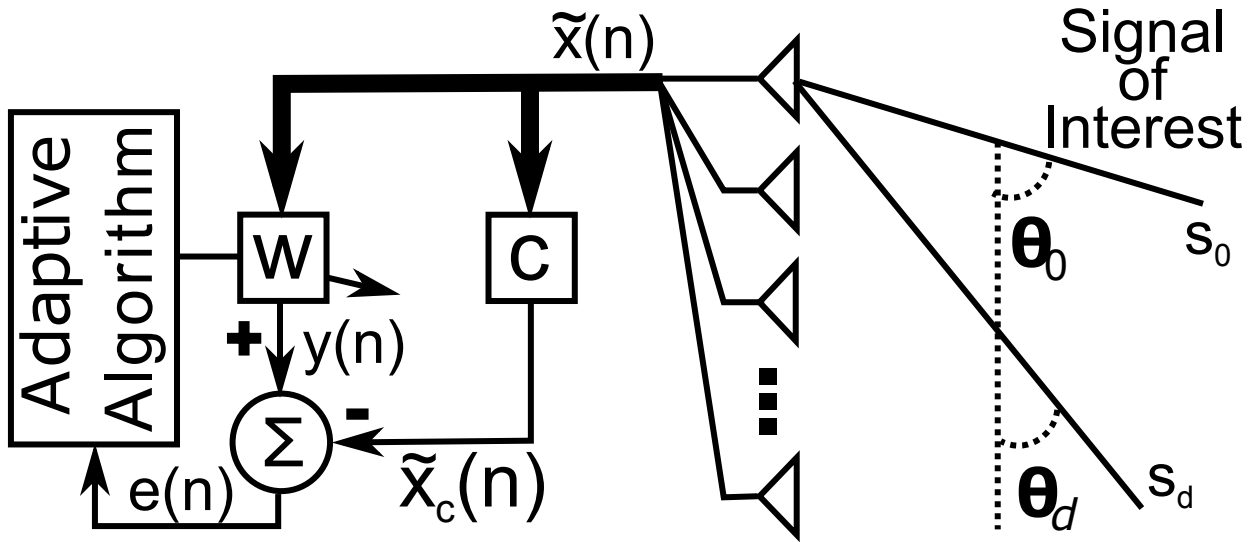


Figure 2.2: Adaptive LCMV filter with its antenna array [3, 4].

Reduced Rank Filters

Reduced Rank filtering, illustrated in Chapter 3, is achieved by an additional filtering stage to the adaptive filter. The rank reduction aims at reducing the redundancy of the antenna array received signal by reducing its dimensions [6, 7]. Since a double stage filtering is performed, the adapting convergence is achieved faster, and with the redundancy reduction, the raw storage needs, for any kind of post processing are reduced as well.

A simplified diagram of the LCMV reduced rank filter is presented in Figure 2.3. The constrained signal have its rank recuded by a transformation matrix, \mathbf{T} , and it is filtered by the reduced rank filter afterwards, represented by $\bar{\mathbf{W}}$. The adaptive algorithm adapts both \mathbf{T} and $\bar{\mathbf{W}}$, in order to achieve a faster convergence.

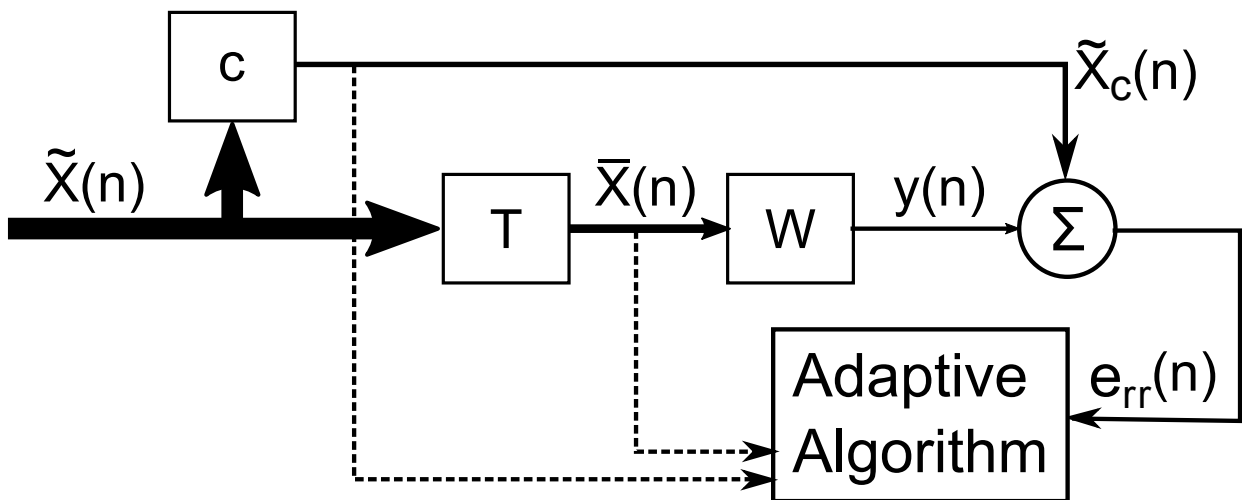


Figure 2.3: Adaptive reduced rank LCMV filter block [5, 3, 6, 7, 8, 9].

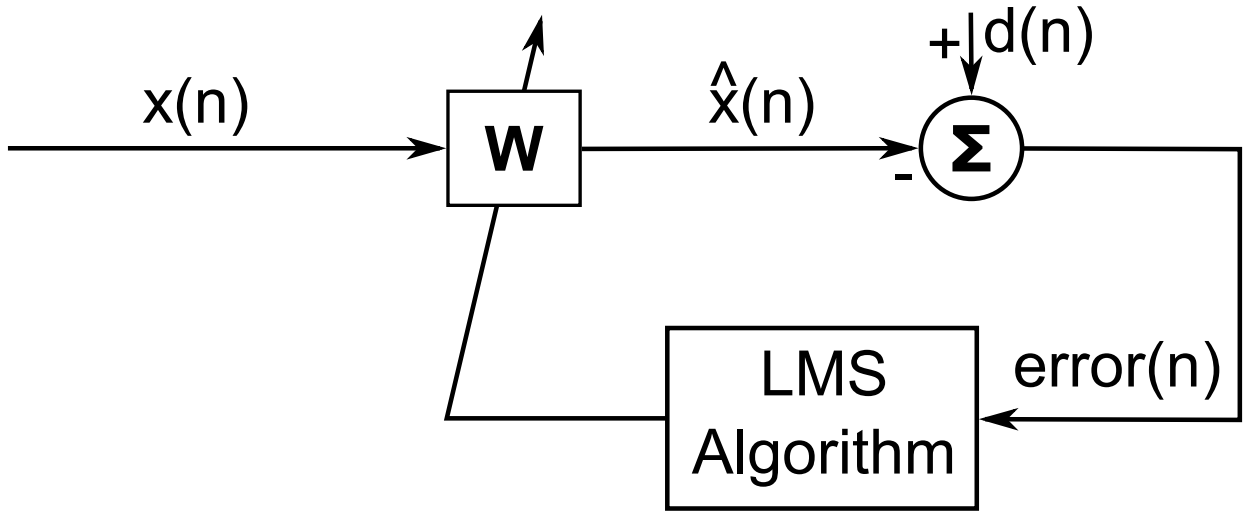


Figure 2.4: Simplified LMS adapting algorithm block [3].

Least Mean Squares Algorithm

The Least Mean Squares (LMS) algorithm, described in Chapter 3, invented by Widrow and Hoff in the 1960's, is an important and widely used technique for adaptive filtering, due its simplicity and low computational cost [3, 19, 6]. The LMS algorithm differs from the Steepest Descent algorithm by using a cost function based on the error's stochastic gradient, instead of a solution based on deterministic values at the Wiener filter output tap [6, 19, 3].

Its function, illustrated in Figure 2.4 with the simplified diagram block is based into two steps:

1. Stochastic error computation between the digital filter taps outputs and the desired signal;
2. Using the computed error in order to compute the stochastic gradient, to adjust the filters weights.

Proposed simulation technique with the Unscented Transform

In this work the low complexity Unscented Transform simulation performance assessment technique with adaptive LCMV and adaptive reduced rank LCMV filters approach is examined. Parameters such as the performance and accuracy are considered in comparison with obtained results from Monte Carlo simulations. The proposed approach is summarized in nine steps, as illustrated in Figure 2.5.

- In ①, the simulation scenario is created, the noise and signals characteristics, such as the noise and signal variances, signal modulation, interferers' variances and the direction of arrivals are considered.
- In ②, the definition of which random variables are critical for the scenario is crucial for the correct functioning and computation of the UT. In this work random variables that have

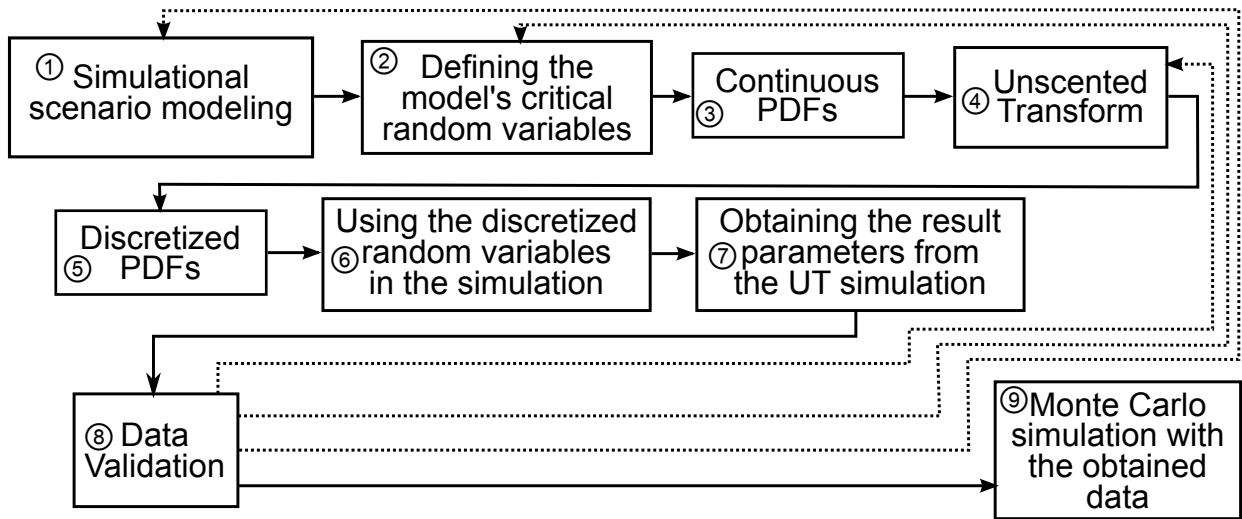


Figure 2.5: Proposed approach chart.

greater impact over the desired signal are considered critical, such as the noise and interferers with variances higher than that of the signal of interest (SOI).

- In ③ and ④ the UT is computed over all critical random variables, in order to obtain a finite set of points.
- In ⑤ and ⑥, a probabilistic set of points is computed by the combination of all points obtained from the UT.
- In ⑦, the results from the UT simulation is obtained.
- At last, in ⑧ and ⑨, the UT simulation is evaluated, comparing its results with a Monte Carlo simulation, considering possible and plausible errors caused by the discretization of continuous random variables.

Proposed digital radioaltimeter

In this work a digital radioaltimeter, that uses a binary-phase-shift keying (BPSK) modulation scheme and LCMV beamformers is presented. The proposed radioaltimeter is capable of modeling its receiving lobe using an LCMV beamformer, in order to separate the non-line-of-sight signals from the line-of-signal and other interferers, in order to estimate the correct airborne system altitude.

Figure 2.6 brings the simplified diagram of the radioaltimeter. The radioaltimeter is comprised of a radio-transmitter and an antenna array radio-receiver. The transmitting signal is a triangle wave which is digitalized by an analog-to-digital converter and modulated by a phase-shift-keying scheme. The backscattered signal impinges the antenna array and is demodulated and LCMV filtered afterwards, in order to beamform the antenna array's receiving lobe. The digital signal processing processor senses the phase shift, caused by the backscattering time delay in order to compute the airborne system altitude.

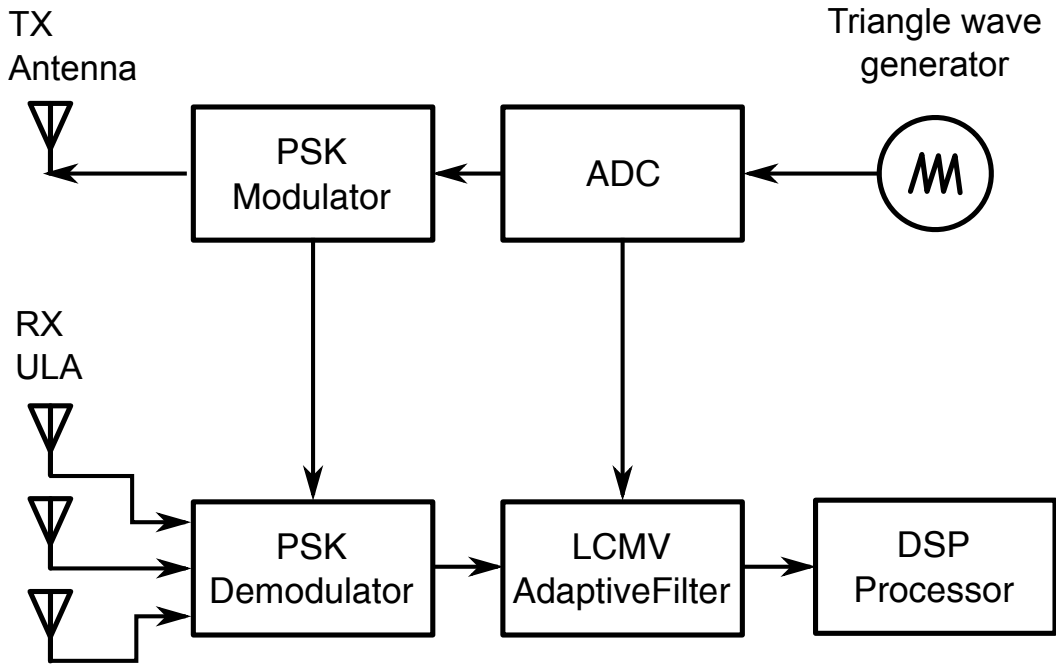


Figure 2.6: Simplified diagram of the proposed radioaltimeter.

Applications

The use of Unscented Transform improves the simulation execution time of stochastic systems by discretizing the continuous random variables, that gives rise to the academic and economic advantage of allowing for technologies and products to enter the market quicker due to a reduced development time.

Reduced rank filters are versatile and, by adding one more filtering stage, improve the convergence time of adaptive filters. With the received signal redundancy reduction, they essentially act like a low loss compression, reducing the raw storage costs and needs, which is important for storing raw signals for post processing and other types of treatments.

The novel digital radioaltimeter presented in this work allows a radioaltimeter estimate the real airborne system altitude by the use of LCMV filtering and binary-phase-shift-keying techniques.

Simulation Results

In order to evaluate the proposed technique, a set of computational simulations is presented in Section 4.6. The full rank LCMV and reduced rank LCMV adaptive filters performance is evaluated in comparison of well known results presented in [4, 7, 20]. The Unscented Transform performance assessment evaluation uses results and techniques derived from [2, 21, 22, 23, 16].

The proposed radioaltimeter simulations are located in Chapter 5.

Contributions

The main contributions of this work is the low complexity Unscented Transform performance assessment for stochastic models and systems simulation, which improves the celerity or, at least a good parameter estimation and basis for Monte Carlo simulations. A novel digital radioaltimeter that uses LCMV beamforming is presented, and this work also evaluates the performance of reduced rank LCMV filters in comparison with full rank LCMV filters.

The assessment of the Unscented Transform is of great value and importance for academic, industrial and commercial scopes and reduced rank filtering has a great practical application in several research branches from mass communication systems to data acquisition in electrical and electronics engineering, geology, mechanics and economic sciences.

Acknowledgments

The author would like to thank the (PVE) project related to satellite communication and navigation supported by the Brazilian government, the Coordination for the Improvement of Higher Education Personnel (CAPES) and the National Council for Scientific and Technological Development (CNPq) under the process number 88881.030392/2013-01 for their financial support on this research.

Chapter 3

Data Model

This chapter is divided into eight sections, in which Section 3.1 brings the notation used in this work while Section 3.2 explains the mathematical concepts of the Kronecker Product and the Kronecker Sum. Section 3.3 introduces the Unscented Transform briefly, with basic probabilistics concepts while Section 3.4 brings the phase-shift keying mathematical explanation, the binary-phase-shift-keying is used in this work, and Section 3.5 presents the data model for LCMV filters and other antenna arrays systems. Section 3.6 details the optimal non-adaptive LCMV filter, in order to give a basis to adaptive LCMV filtering, and Section 3.7 shows the LCMV adaptive filter solution. Finally, Section 3.8 presents the adaptive solution for the reduced rank LCMV filter.

3.1 Notation

This work uses the following notation to represent scalars and matrices: Scalars are denoted by italic lowercase letters (a, b, \dots), column vectors as boldface lowercase letters and matrices as boldface uppercase letters ($\mathbf{a}, \mathbf{b}, \dots, \mathbf{A}, \mathbf{B}, \dots$). The (i, j) -element of the matrix \mathbf{A} , is denoted as a_{ij} . The probability function, modulus operator, intersection operator, union operator, Hermitian transpose, matrix transpose and complex conjugate are represented by $p(\cdot)$, $|\cdot|^2$, \cap , \cup , $(\cdot)^H$, $(\cdot)^T$ and $(\cdot)^*$, respectively. Mathematical complex, real and imaginary domains are denoted by \mathbb{C} , \mathbb{R} and \mathbb{Q} , respectively.

The operator $\text{diag}(\cdot)$ is the diagonalization operator, where a non-diagonal matrix is turned into a diagonal matrix, and the $\text{dediag}(\cdot)$ operator constructs a vector from the main diagonal of a matrix.

3.2 Kronecker operators

The Kronecker sum [24], denoted by \oplus , is characterized by the sum of two square matrices in which the resulting matrix diagonal forms a combinatorial sum of all elements of the both matrices [24].

3.2.1 Kronecker Product

To explain the concept of the Kronecker Product [25], let $\mathbf{\Delta}$ be a $m \times n$ matrix and $\mathbf{\Upsilon}$, an $i \times j$ matrix. The Kronecker product, denoted by \otimes , which is also called the matrix direct product [25] results into a $(m.i) \times (n.j)$ $\mathbf{\Gamma}$ matrix, $\mathbf{\Gamma} = \mathbf{\Delta} \otimes \mathbf{\Upsilon}$, as follows:

$$\mathbf{\Gamma} = \mathbf{\Delta} \otimes \mathbf{\Upsilon} = \begin{pmatrix} \delta_{11}\mathbf{\Upsilon} & \delta_{12}\mathbf{\Upsilon} & \cdots & \delta_{1n}\mathbf{\Upsilon} \\ \delta_{21}\mathbf{\Upsilon} & \delta_{22}\mathbf{\Upsilon} & \cdots & \delta_{2n}\mathbf{\Upsilon} \\ \vdots & \vdots & \ddots & \vdots \\ \delta_{m1}\mathbf{\Upsilon} & \delta_{m2}\mathbf{\Upsilon} & \cdots & \delta_{mn}\mathbf{\Upsilon} \end{pmatrix}. \quad (3.1)$$

3.2.2 Kronecker Sum

Let $\mathbf{\Gamma} = \mathbf{\Delta} \oplus \mathbf{\Upsilon}$ be the Kronecker sum of a two square matrices, $\mathbf{\Delta}$ and $\mathbf{\Upsilon}$:

$$\mathbf{\Gamma} = \mathbf{\Delta} \oplus \mathbf{\Upsilon} = \mathbf{\Delta} \otimes \mathbf{I}_{\mathbf{\Upsilon}} + \mathbf{I}_{\mathbf{\Delta}} \otimes \mathbf{\Upsilon}, \quad (3.2)$$

where \otimes is the Kronecker product [25], $\mathbf{I}_{\mathbf{\Upsilon}}$ and $\mathbf{I}_{\mathbf{\Delta}}$ are the identity matrices with the same sizes of $\mathbf{\Upsilon}$ and $\mathbf{\Delta}$, respectively. Solving (3.2), yields a $\mathbf{\Gamma}$ block matrix comprised by a set of $m \times n$ matrices:

$$\begin{aligned} \mathbf{\Gamma} &= \mathbf{\Delta} \otimes \mathbf{I}_{\mathbf{\Upsilon}} + \mathbf{I}_{\mathbf{\Delta}} \otimes \mathbf{\Upsilon} = \\ & \begin{pmatrix} \delta_{11}\mathbf{I}_{\mathbf{\Upsilon}} & \delta_{12}\mathbf{I}_{\mathbf{\Upsilon}} & \cdots & \delta_{1m}\mathbf{I}_{\mathbf{\Upsilon}} \\ \delta_{21}\mathbf{I}_{\mathbf{\Upsilon}} & \delta_{22}\mathbf{I}_{\mathbf{\Upsilon}} & \cdots & \delta_{2m}\mathbf{I}_{\mathbf{\Upsilon}} \\ \vdots & \vdots & \ddots & \vdots \\ \delta_{m1}\mathbf{I}_{\mathbf{\Upsilon}} & \delta_{m2}\mathbf{I}_{\mathbf{\Upsilon}} & \cdots & \delta_{mm}\mathbf{I}_{\mathbf{\Upsilon}} \end{pmatrix} + \begin{pmatrix} \mathbf{I}_{\mathbf{\Delta}}\mathbf{\Upsilon}_{11} & \mathbf{I}_{\mathbf{\Delta}}\mathbf{\Upsilon}_{12} & \cdots & \mathbf{I}_{\mathbf{\Delta}}\mathbf{\Upsilon}_{1n} \\ \mathbf{I}_{\mathbf{\Delta}}\mathbf{\Upsilon}_{21} & \mathbf{I}_{\mathbf{\Delta}}\mathbf{\Upsilon}_{22} & \cdots & \mathbf{I}_{\mathbf{\Delta}}\mathbf{\Upsilon}_{2n} \\ \vdots & \vdots & \ddots & \vdots \\ \mathbf{I}_{\mathbf{\Delta}}\mathbf{\Upsilon}_{n1} & \mathbf{I}_{\mathbf{\Delta}}\mathbf{\Upsilon}_{n2} & \cdots & \mathbf{I}_{\mathbf{\Delta}}\mathbf{\Upsilon}_{nn} \end{pmatrix} = \\ & \begin{pmatrix} \left. \begin{array}{ccc} \delta_{11+v_{11}} & \cdots & \varpi \\ \vdots & \ddots & \vdots \\ \varpi & \cdots & \delta_{11+v_{nn}} \end{array} \right| \Pi & \cdots & \Pi \\ \vdots & \ddots & \vdots \\ \Pi & \Pi & \cdots \left. \begin{array}{ccc} \delta_{mm+v_{nn}} & \cdots & \varpi \\ \vdots & \ddots & \vdots \\ \varpi & \cdots & \delta_{mm+v_{nn}} \end{array} \right| \end{pmatrix}, \quad (3.3) \end{aligned}$$

where Π is comprised by generic ϖ elements, is an unwanted matrix and elements, in the scope of this paper, as illustrated in Subsection 3.2.3.

3.2.3 Kronecker sum of vectors

Let $\mathbf{\Gamma} = \delta \oplus v$ be the Kronecker Sum of two vectors, a $\delta \in \mathbb{C}^{1 \times m}$ vector and a $v \in \mathbb{C}^{1 \times n}$ vector.

In order to apply the Kronecker sum according to Eq. (3.2), the $\text{diag}(\cdot)$ operator should be first applied to the vectors δ and v , since the Kronecker Sum can only be executed with square matrices [24]:

$$\mathbf{\Gamma} = \text{dediag}[\text{diag}(\delta) \oplus \text{diag}(v)], \quad (3.4)$$

$$\text{diag}(\delta) = \begin{pmatrix} \delta_1 & 0 \\ 0 & \delta_m \end{pmatrix}, \quad (3.5)$$

$$\text{diag}(v) = \begin{pmatrix} v_1 & 0 \\ 0 & v_m \end{pmatrix}, \quad (3.6)$$

where $\text{diag}(\cdot)$ is the diagonalization and $\text{dediag}(\cdot)$ is de-diagonalization operator. By executing the Kronecker Sum, as stated in (3.2), we obtain:

$$\mathbf{\Gamma} = \begin{pmatrix} \delta_1 + v_1 & 0 & 0 & 0 & 0 & 0 & 0 & 0 \\ 0 & \ddots & 0 & 0 & 0 & 0 & 0 & 0 \\ 0 & 0 & \delta_1 + v_n & 0 & 0 & 0 & 0 & 0 \\ 0 & 0 & 0 & \delta_2 + v_2 & 0 & 0 & 0 & 0 \\ 0 & 0 & 0 & 0 & \ddots & 0 & 0 & 0 \\ 0 & 0 & 0 & 0 & 0 & \delta_2 + v_n & 0 & 0 \\ 0 & 0 & 0 & 0 & 0 & 0 & \ddots & 0 \\ 0 & 0 & 0 & 0 & 0 & 0 & 0 & \delta_m + v_n \end{pmatrix}, \quad (3.7)$$

$$\begin{aligned} \text{dediag}(\mathbf{\Gamma}) = \\ [\delta_1 + v_1 \dots \delta_1 + v_n \delta_2 + v_1 \dots \delta_2 + v_n \dots \delta_m + v_1 \dots \delta_m + v_n], \end{aligned} \quad (3.8)$$

which results in a combinatorial sum of all arrays elements.

3.3 Unscented Transform

The UT maps and discretizes a continuous probability distribution (PDF), mainly, by calculating its statistical moments [2, 1]. The discretized PDF must have the same or very close statistical moments [16, 1, 2, 8, 9]. The advantage of a discrete PDF over a continuous PDF is the reduced set of points, which improves the speed of simulation execution.

In the UT discrete PDF, we define the Sigma points as the random variables (RV) and the weight points as their probabilities.

The n -th moment of a continuous \mathbf{X} -RV PDF, with probability $p(\mathbf{X})$, is defined as [13, 12]:

$$\mathbf{E}[\mathbf{X}^n] = \int_{-\infty}^{\infty} \mathbf{X}^n p(\mathbf{X}) d\mathbf{X}. \quad (3.9)$$

The UT discrete non-linear mapping creates a discrete PDF with a set of z Sigma points, $\Phi = [\phi_1, \phi_2, \dots, \phi_z]$, and $\Psi = p(\Phi)$ weight points, using a Taylor expansion, that must satisfy the conditions as follows [2, 1]:

$$\begin{aligned} \mathbf{E}_{\text{continuous}}[\mathbf{X}^n] &\equiv \mathbf{E}_{\text{discrete}}[\Phi^n], \\ \int_{-\infty}^{\infty} \mathbf{X}^n p(\mathbf{X}) d\mathbf{X} &\equiv \sum_{k=1}^z \phi_k^z \psi_k \equiv \\ &\sum_{k=1}^z \mathbf{X}^n \psi_k \delta(\mathbf{X} - \phi_k), \end{aligned} \quad (3.10)$$

where the continuous PDF is \mathbf{X} , the discretized PDF is Φ and $\delta(\cdot)$ is the unitary impulse function, resembling the sampling theorem [26].

3.4 Phase Shift Keying modulation

Phase Shift Keying (PSK) is a type of digital modulation in which each signal bit has a corresponding phase, which can be generalized to the following mathematical expression [26, 27]:

$$\varphi_{\text{PSK}} = \frac{2\pi}{m}, \quad (3.11)$$

where φ_{PSK} is the phase interval of each bit from the m -ary bit coded signal, therefore a digital constellation of m points, leading to a set of m phases for the modulation with a φ_{offset} phase offset:

$$\Phi_{\text{PSK}} = \varphi_{\text{offset}} + \left[\frac{2\pi}{m}, \frac{4\pi}{m}, \frac{6\pi}{m}, \dots, 2\pi \right]. \quad (3.12)$$

Leading to a generalized m -PSK expression, assuming a uniformly distributed set of bits and signal variance of $\sigma_{m\text{-PSK}}^2$:

$$\mathbf{S}_{m\text{-PSK}} = \frac{\sigma_{m\text{-PSK}}}{\sqrt{m}} [e^{j\Phi_{\text{PSK}}(1)}, e^{j\Phi_{\text{PSK}}(2)}, e^{j\Phi_{\text{PSK}}(3)}, \dots, e^{j\Phi_{\text{PSK}}(m)}].$$

3.4.1 Binary PSK modulation

The binary PSK (BPSK) modulation is a PSK modulation in which the signal is coded into two bits, yielding a digital constellation, shown in Figure 3.1, of two phases, for a zero-offset phase BPSK signal we have:

$$\Phi_{\text{BPSK}} = [\pi, 2\pi]. \quad (3.13)$$

$$\mathbf{S}_{\text{BPSK}} = \frac{\sigma_{\text{BPSK}}}{\sqrt{2}} [e^{-j\pi}, e^{-j2\pi}], \quad (3.14)$$

$$\mathbf{S}_{\text{BPSK}} = \frac{\sigma_{\text{BPSK}}}{\sqrt{2}} [-1, +1]. \quad (3.15)$$

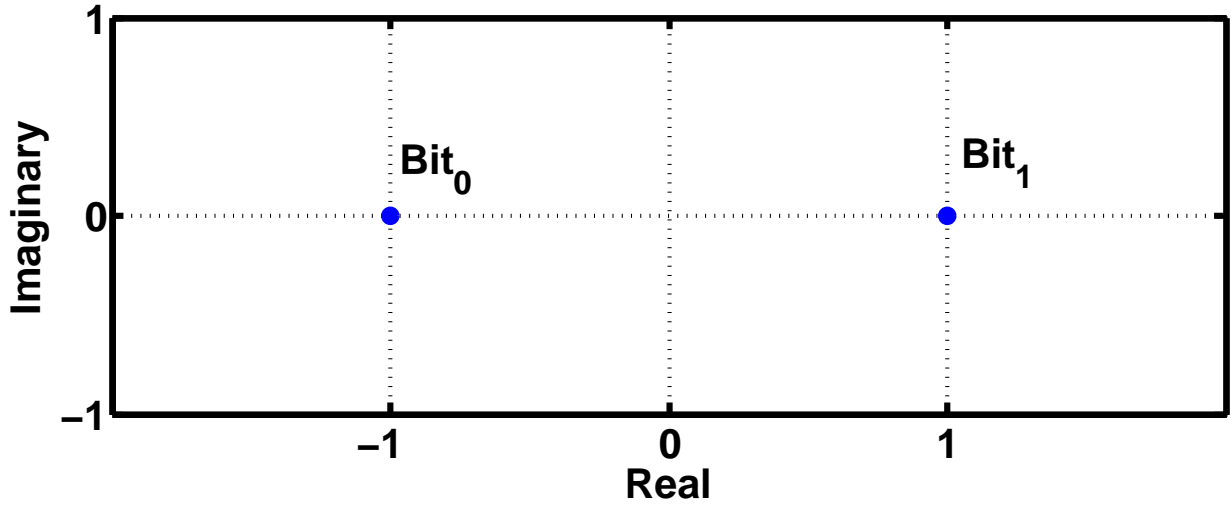


Figure 3.1: BPSK constellation.

3.5 Data Model for LCMV filters

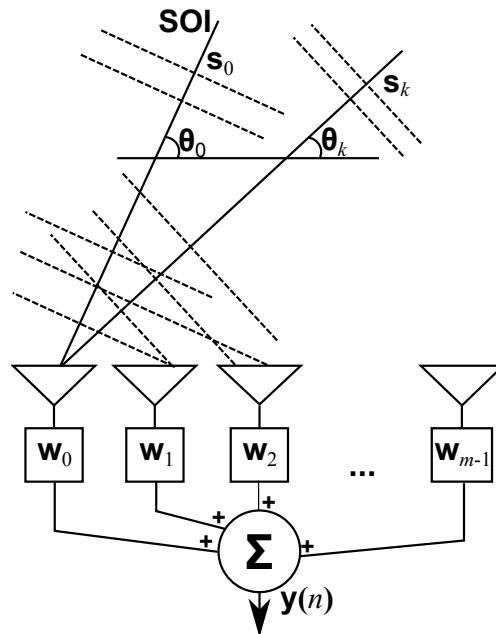


Figure 3.2: Simplified block of an ULA and LCMV filter[6, 3].

The LCMV can be applied to beamform a antenna array comprised of m sensors, spaced by $\frac{\lambda}{2}$

wavelength, and d impinging signals, as depicted in Figure 3.2. The goal of the LCMV is to find the filter weights $\mathbf{W} = [\mathbf{w}_0, \mathbf{w}_1, \dots, \mathbf{w}_{m-1}]$ in order to maximize the power of the signal of interest (SOI) and reduce the interference from the other directions.

According to Figure 3.2, the filter output for each sample is $y(n)$, so that the filter output can be rewritten as:

$$y(n) = \mathbf{w}^H \mathbf{x}, \quad (3.16)$$

where the filter input, $\mathbf{x} \in \mathbb{C}^{m \times 1}$, is:

$$\mathbf{x} = \mathbf{A} \mathbf{s} + \mathbf{n}. \quad (3.17)$$

We define \mathbf{A} as the steering matrix, comprised of d steering vectors of size $1 \times m$:

$$\mathbf{A} = [\mathbf{a}(\theta_0), \mathbf{a}(\theta_1), \dots, \mathbf{a}(\theta_d)], \quad (3.18)$$

where:

$$\mathbf{a}(\theta_d) = [1, e^{j\pi \cdot \lambda \cdot \cos(\theta_d)}, \dots, e^{j\pi \cdot \lambda \cdot \cos(\theta_d)(m-1)}]^T. \quad (3.19)$$

Implying in:

$$\mathbf{A} = \begin{pmatrix} 1 & e^{j2\pi \cdot \lambda \cdot \cos(\theta_0)} & \dots & e^{j2\pi \cdot \lambda \cdot \cos(\theta_0) \cdot (m-1)} \\ 1 & e^{j2\pi \cdot \lambda \cdot \cos(\theta_1)} & \dots & e^{j2\pi \cdot \lambda \cdot \cos(\theta_1) \cdot (m-1)} \\ \vdots & \vdots & \ddots & \vdots \\ 1 & e^{j2\pi \cdot \lambda \cdot \cos(\theta_k)} & \dots & e^{j2\pi \cdot \lambda \cdot \cos(\theta_k) \cdot (m-1)} \end{pmatrix}^T \quad (3.20)$$

\mathbf{s} is a set of d impinging signals on a uniform linear array (ULA) of antennas.

$$\mathbf{s} = [s_0(n) \ s_1(n) \ s_2(n) \ \dots \ s_{d-1}(n)]^T. \quad (3.21)$$

Each signal has a variance, in which the interfering signals have a $[\sigma_{\mathbf{s},k}^2]_{k=1}^d = \sigma_{\mathbf{s},\text{INT}}^2$ variance and a direction of arrival (DOA), θ_d and the SOI have a $\sigma_{\mathbf{s},0}^2 = \sigma_{\mathbf{s},\text{SOI}}^2$ variance, and θ_0 , for the sake of simplicity, is the SOI DOA; \mathbf{n} is the complex additive white Gaussian noise (AWGN) vector, with $\sigma_{\mathbf{n}}^2$ variance, where $\mathbf{n} = \frac{\sigma_{\mathbf{n}}}{\sqrt{2}}(\mathbf{n} + j\mathbf{n})$, in that we rewrite (3.17) and (3.16) as in [5]:

$$\mathbf{x}(n) = \mathbf{a}(\theta_0)s_0(n) + \mathbf{A}_{\text{int}}\mathbf{s}_{\text{int}} + \mathbf{n}, \quad (3.22)$$

$$y(n) = \mathbf{w}^H[\mathbf{a}(\theta_0)s_0(n) + \mathbf{A}_{\text{int}}\mathbf{s}_{\text{int}} + \mathbf{n}], \quad (3.23)$$

where \mathbf{A}_{int} and \mathbf{S}_{int} are the interferers' steering matrix, containing the interfering signals' DOAs and the interferers' transmitted symbol matrix, respectively.

3.6 Non-adaptive LCMV filters

As stated in Section 3.5 the LCMV filter minimizes the array's output signal energy, which yields the filter's cost function and constraint:

$$J_{\text{LCMV-LMS}} = \mathbf{E}[|y(n)|^2] = \mathbf{E}[\mathbf{w}^H\mathbf{x}(n)\mathbf{x}(n)^H\mathbf{w}], \quad (3.24)$$

$$\text{s.t. } \sum_{j=0}^{m-1} c_j \cdot w_j = f. \quad (3.25)$$

Where \mathbf{c} is the LCMV constraint array and f is the gain, which is usually unity. The constraint for the constraint array is the signal of interest (SOI) steering vector, which can be obtained from the corresponding line of the steering matrix \mathbf{A} . Since the noise is assumed to be uncorrelated to the signal itself, $\mathbf{E}[\mathbf{x}(n)\mathbf{n}^H] = 0$, therefore the noise related members are omitted.

Using the Lagrange's multipliers, the constrained cost function minimization can be rewritten [3, 6]:

$$J_{\text{LCMV-LMS}} = \mathbf{E}[|y(n)|^2] + \Lambda(\mathbf{c}^H\mathbf{w} - f), \quad (3.26)$$

$$J_{\text{LCMV-LMS}} = \mathbf{E}[\mathbf{w}^H\mathbf{x}(n)\mathbf{x}(n)^H\mathbf{w}] + \Lambda(\mathbf{c}^H\mathbf{w} - f), \quad (3.27)$$

$$J_{\text{LCMV-LMS}} = \mathbf{E}[\mathbf{w}^H\mathbf{R}_{\text{XX}}\mathbf{w}] + \Lambda(\mathbf{c}^H\mathbf{w} - f), \quad (3.28)$$

yielding a gradient with respect to \mathbf{w} [6, 3]:

$$\mathbf{g}\mathbf{w} = 2\mathbf{R}_{\text{XX}}\mathbf{w} + \Lambda\mathbf{c}, \quad (3.29)$$

where \mathbf{R}_{XX} is the signal definite and positive auto-correlation matrix defined as $\mathbf{E}[\mathbf{x}(n)\mathbf{x}^H(n)]$.

A unique $\mathbf{w} = \mathbf{w}_{\text{optimal}}$ will satisfy the condition $\mathbf{g}\mathbf{w} = \mathbf{0}$, which minimizes ξ_c [6, 3], solving the gradient:

$$2\mathbf{R}_{\text{XX}}\mathbf{w}_{\text{optimal}} + \Lambda\mathbf{c} = 0, \quad (3.30)$$

$$2\mathbf{w}_{\text{optimal}} + \Lambda\mathbf{c}^H\mathbf{R}_{\text{XX}}^{-1}\mathbf{c} = 0, \quad (3.31)$$

$$2f + \mathbf{c}^H\mathbf{R}_{\text{XX}}^{-1}\mathbf{c} = 0, \quad (3.32)$$

$$\Lambda = -\frac{2f}{\mathbf{c}^H\mathbf{R}_{\text{XX}}^{-1}\mathbf{c}}, \quad (3.33)$$

yielding the optimal LCMV filter:

$$\mathbf{w}_{\text{optimal}} = \frac{\mathbf{R}_{\mathbf{xx}}^{-1} \mathbf{c} f}{\mathbf{c}^H \mathbf{R}_{\mathbf{xx}}^{-1} \mathbf{c}}, \quad (3.34)$$

which can be set to the unitary gain, as follows:

$$\mathbf{w}_{\text{optimal,unitary}} = \frac{\mathbf{R}_{\mathbf{xx}}^{-1} \mathbf{c}}{\mathbf{c}^H \mathbf{R}_{\mathbf{xx}}^{-1} \mathbf{c}}. \quad (3.35)$$

Equation (3.35) is the closed solution, which is non-adaptive and is deterministic, it does not cater for significant variations in the incoming signal auto correlation nor in the noise, neither in the interferers.

3.7 LCMV-LMS adaptive filters

In real scenarios, the SOI, interferers and noise are always changing, so for a practical application the filter must adapt to these changes. In the scope of this work the LMS algorithm is used for the reasons exposed on Section 3.7.

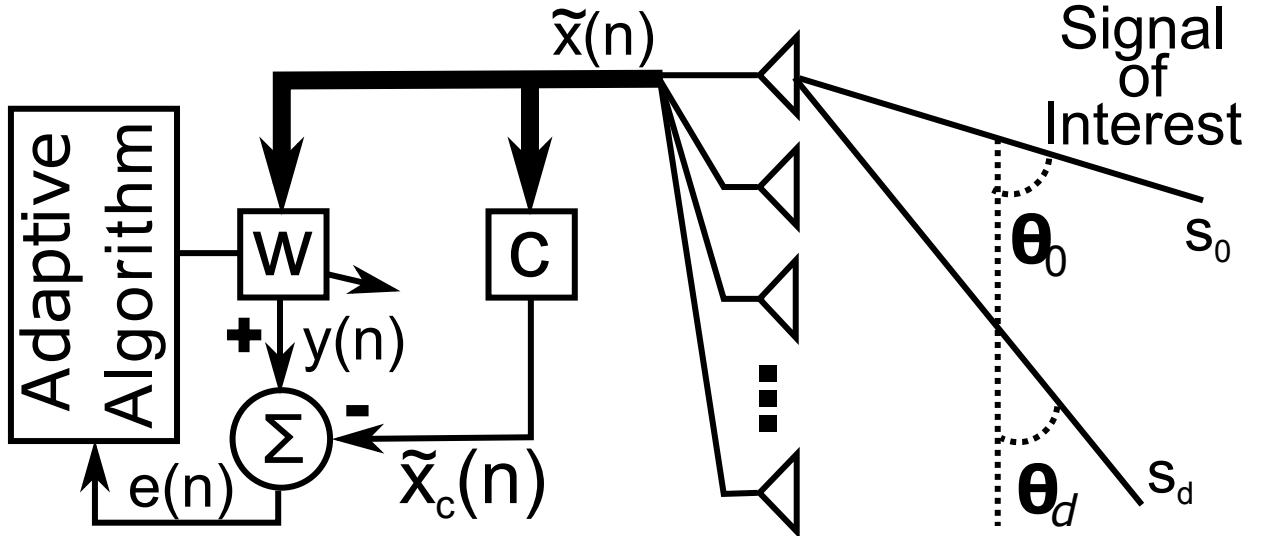


Figura 3.3: LCMV adaptive filter [3, 4].

The Wiener solution for a minimum mean-square error (MMSE) in estimating the constrained signal $\tilde{x}_c(n)$ is given by [6]:

$$\mathbf{w}_{\text{optimal}} = \mathbf{R}_{\mathbf{xx}}^{-1} \mathbf{p} \quad (3.36)$$

where $\mathbf{p} = \mathbf{E}[\tilde{x}_c(n) \tilde{\mathbf{x}}(n)]$, an estimate of the current samples of the incoming signal and the expected

signal. It is assumed that $\tilde{x}_{\mathbf{c}}(n)$ and $\mathbf{x}(n)$ are jointly wide-sense stationary (JWSS) [3, 12].

An algorithm based on the steepest-descent solution is used, based on the fact that good estimates of the auto correlation matrix, $\mathbf{R}_{\mathbf{xx}}$, and the constant p , denoted by $\hat{\mathbf{R}}_{\mathbf{xx}}(n)$ and $\hat{p}(n)$, respectively are available [3, 6]:

$$\mathbf{w}(n+1) = \mathbf{w}(n) - \mu \hat{\mathbf{g}}_{\mathbf{w}}(n) \quad (3.37)$$

$$\mathbf{w}(n+1) = \mathbf{w}(n) + 2\{\mu \hat{p}(n) - \hat{\mathbf{R}}_{\mathbf{xx}}(n)\mathbf{w}(n)\} \quad (3.38)$$

Since we are dealing with adaptive filtering, the n -th samples can be used to obtain estimates for $\mathbf{R}_{\mathbf{xx}}$ and p [6]:

$$\hat{\mathbf{R}}_{\mathbf{xx}}(n) = \mathbf{E}[\tilde{\mathbf{x}}(n)\tilde{\mathbf{x}}^H(n)] = \tilde{\mathbf{x}}(n)\tilde{\mathbf{x}}^H(n) \quad (3.39)$$

$$\hat{p}(n) = \mathbf{E}[\tilde{x}_{\mathbf{c}}(n)\tilde{\mathbf{x}}(n)] = \tilde{x}_{\mathbf{c}}(n)\tilde{\mathbf{x}}(n) \quad (3.40)$$

yielding the stochastic error gradient for the current signal sample [3, 6]:

$$\hat{\mathbf{g}}_{\mathbf{w}}(n) = -2\tilde{\mathbf{x}}(n)(\tilde{x}_{\mathbf{c}}(n)\tilde{\mathbf{x}}(n) + \tilde{\mathbf{x}}^H(n)\mathbf{w}(n)) \quad (3.41)$$

$$\hat{\mathbf{g}}_{\mathbf{w}}(n) = -2e(n)\tilde{\mathbf{x}}(n) \quad (3.42)$$

This gives us the LMS algorithm update rate equation[3, 6]:

$$\mathbf{w}(k+1) = \mathbf{w}(n) + 2\mu e^*(n)\tilde{\mathbf{x}}(n) \quad (3.43)$$

where $e(n) = \tilde{x}_{\mathbf{c}}(n) - \mathbf{w}^H(n)\tilde{\mathbf{x}}(n)$.

The LMS algorithm depends upon the convergence factor, μ , which can be chosen between $0 < \mu < \frac{1}{\text{tr}[\mathbf{R}_{\mathbf{xx}}]}$ [6], using the trace operator.

3.8 Reduced rank LCMV-LMS adaptive filters

The adaptive LCMV filter in this work, illustrated in Figure 3.4, uses the Reduced Rank LMS algorithm to perform the filter adaptation. The LMS algorithm is widely used in adaptive filtering processes, specially due its low computational demands [6, 3].

An LCMV filter minimizes the array's output signal energy for non-constrained signals [6, 3]:

$$\mathbf{E}[|y(n)|^2] = \mathbf{E}[\mathbf{w}^H \mathbf{x}(n) \mathbf{x}(n)^H \mathbf{w}], \text{ s.t. } \mathbf{a}^H(\theta_0) \cdot \mathbf{w} = g \quad (3.44)$$

where $\mathbf{c} = \mathbf{a}(\theta_0)$ is the LCMV array constraint and g is the desired gain, which, for the sake of the simplicity, is unity [6, 3].

As illustrated in Figure 3.4 the received signal, $\tilde{\mathbf{x}}(n) \in \mathbb{C}^{m \times 1}$, is subject to a constraint vector

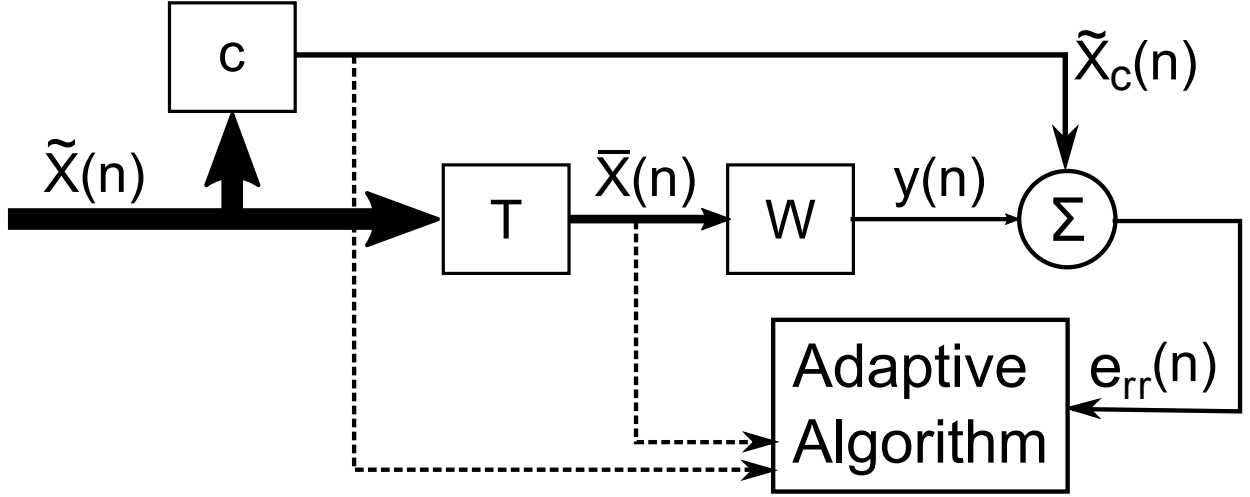


Figure 3.4: Diagram block of a reduced rank LCMV adaptive filter [5, 3, 6, 7, 9, 8].

\mathbf{c} , containing the SOI DOA yielding the constrained signal $\tilde{x}_c(n) = \mathbf{c}^H \tilde{\mathbf{x}}(n)$.

The rank reduction is performed by an $m \times \alpha$ projection matrix, \mathbf{T} , where $\alpha < m$, yielding the reduced rank versions of the signal [7, 5, 9, 8]:

$$\bar{\mathbf{x}}(n) = \mathbf{T}^H(n) \tilde{\mathbf{x}}(n), \quad (3.45)$$

$$y(n) = \bar{\mathbf{w}}^H(n) \bar{\mathbf{x}}(n), \quad (3.46)$$

where $\bar{\mathbf{x}}(n) \in \mathbb{C}^{\alpha \times 1}$ and $\bar{\mathbf{w}}(n) \in \mathbb{C}^{\alpha \times 1}$ are the reduced rank versions of the system variables.

The Reduced Rank LMS works by adapting the weight vector, $\bar{\mathbf{w}}$, and the projection matrix, \mathbf{T} , both subject to the LCMV beamforming condition in (3.44). Solving the cost function of stochastic gradient [5, 9, 8], found in Wiener solution [6, 3], we obtain:

$$J_{\text{RR-LMS}}(\mathbf{w}, \mathbf{T}) = \mathbf{E}[|\tilde{x}_c(n) - \bar{\mathbf{w}}^H \bar{\mathbf{x}}(n)|^2] \quad (3.47)$$

yielding the adaptive part updating rule with μ steps [5, 20, 4, 7, 9, 8]:

$$\bar{\mathbf{w}}(n+1) = \bar{\mathbf{w}}(n) - \mu \nabla_{\mathbf{w}} J_{\text{RR-LMS}}(\bar{\mathbf{w}}), \quad (3.48)$$

$$\bar{\mathbf{w}}(n+1) = \bar{\mathbf{w}}(n) + 2\mu(\tilde{x}_c(n) - \bar{\mathbf{w}}^H \bar{\mathbf{x}}(n))^* \bar{\mathbf{x}}(n), \quad (3.49)$$

$$\mathbf{T}(n+1) = \mathbf{T}(n) - \mu \nabla_{\mathbf{T}} J_{\text{RR-LMS}}(\mathbf{T}) \quad (3.50)$$

$$\mathbf{T}(n+1) = \mathbf{T}(n) + 2\mu \tilde{x}_c(n) (\tilde{x}_c(n) - \bar{\mathbf{w}}^H \bar{\mathbf{x}}(n))^* \bar{\mathbf{w}}(n), \quad (3.51)$$

where $e_{rr}(n) = (y(n) - \tilde{x}_c(n))$, $\mathbf{w}(n) = \mathbf{c} - \mathbf{c}^H \mathbf{T}(n) \bar{\mathbf{w}}(n)$ and instantaneous estimate for $\hat{\mathbf{R}}_{\mathbf{xx}} = \tilde{\mathbf{x}}(n) \tilde{\mathbf{x}}^H(n)$ [5, 9, 8].

Chapter 4

Unscented Transform

This Chapter presents a complete mathematical and stochastic explanation for the Unscented Transform along with simulation results. It is divided into six Sections: Section 4.1 brings the generalization of stochastic models for computer simulations and explains how the Monte Carlo simulation convergence is achieved; Section 4.2 introduces how the Unscented Transform works and explains how its convergence is achieved; Section 4.3 brings a theoretical explanation of the Unscented Transform; Section 4.4 compares, using computational simulations, the Monte Carlo versus the UT convergence; Section 4.5 explains parametrically how the UT can be prepared for computer simulations, finally Section 4.6 shows the simulation results obtained when comparing Monte Carlo and UT simulations, with full-rank and reduced-rank LCMV filters.

4.1 Generalization of stochastic models and Monte Carlo simulations

Let $\boldsymbol{\Omega} = [\boldsymbol{\Omega}_1, \boldsymbol{\Omega}_2, \dots, \boldsymbol{\Omega}_\rho]$ be a set of ρ random variables (RV). Since the Monte Carlo (MC) convergence is based on arithmetic mean of all iterations [12], for a i -iteration MC simulation we define the k -th MC iteration as $\mathbf{f}_k(\boldsymbol{\Omega})$ as the simulation result before the convergence, as follows:

$$[\mathbf{f}_k(\boldsymbol{\Omega})]_{k=1}^i = [\boldsymbol{\Lambda}_k]_{k=1}^i, \quad (4.1)$$

where $\boldsymbol{\Lambda}_k$ is the set of stochastic results found for the k -th MC iteration. In order to calculate the final MC result the following computation is usually applied [12, 13]:

$$\mathbf{F}(\boldsymbol{\Omega}) \equiv \frac{1}{i} \sum_{k=1}^i \mathbf{f}_k(\boldsymbol{\Omega}) \equiv \frac{1}{i} \sum_{k=1}^i \boldsymbol{\Lambda}_k. \quad (4.2)$$

Since all MC iterations have the same weight, the final MC result is calculated by arithmetic mean of all iterations. The final result of a MC simulation after the convergence, within a given confidence interval, as $\mathbf{F}(\boldsymbol{\Omega})$, can be generalized by the probability of the k -th $\mathbf{f}_k(\boldsymbol{\Omega})$ iteration to

be run times the k -th $\mathbf{\Lambda}_k$ result set to be calculated, resulting in an expectancy computation:

$$\mathbf{F}(\mathbf{\Omega}) \equiv \mathbf{E}[\mathbf{\Lambda}_k]_{k=1}^i, \quad (4.3)$$

$$\mathbf{F}(\mathbf{\Omega}) \equiv \sum_{k=1}^i p(\mathbf{\Lambda}_k) \mathbf{\Lambda}_k \quad (4.4)$$

where:

$$p(\mathbf{\Lambda}_1) = p(\mathbf{\Lambda}_2) = \dots = p(\mathbf{\Lambda}_k) = \frac{1}{i}. \quad (4.5)$$

To calculate the τ -th statistical moment for the n -th RV, based on (3.9) and by (4.4), the MC simulation final result is the approximation of $\mathbf{E}[\mathbf{\Omega}_n^\tau]$ within a desired confidence interval:

$$\mathbf{F}(\mathbf{\Omega}_n) = \sum_{k=1}^i p(\mathbf{\Lambda}_{n,i}) \mathbf{\Lambda}_{n,i}^\tau. \quad (4.6)$$

With one iteration, $\mathbf{F}(\mathbf{\Omega}_n) = \mathbf{\Lambda}_n^\tau$, yielding a random value, not the desired result. When $i \rightarrow \infty$, then (4.6) is equal to $\mathbf{E}[\mathbf{\Omega}_n^\tau]$, as it is the Riemann sum [15, 9, 8] with infinite terms. To obtain satisfactory results and a convergence within a good confidence interval, a huge number of iterations are required [13, 12]. Therefore, there is a trade-off between accuracy of the MC performance assessment and the time until convergence.

4.2 Unscented Transform prelude

When using the UT, all critical continuous PDFs in the simulation must be discretized creating a finite set of points. The final simulation result is the global expectancy, while in a Monte Carlo simulation, as in (4.4), the final simulation result is the global average [2, 1, 9, 8].

By applying the UT, each n -th discrete RV, within the $\mathbf{\Omega}$ set described in Subsection 4.1, contains ζ_n Sigma points and ζ_n weight points, where the Sigma points set is:

$$\mathbf{\Phi}_n = [\phi_n(1), \dots, \phi_n(\zeta_n)], \quad (4.7)$$

and the weight points set is:

$$p(\mathbf{\Phi}_n) = \mathbf{\Psi}_n = [\psi_n(1), \dots, \psi_n(\zeta_n)]. \quad (4.8)$$

The total number of iterations required to run the UT simulation, ζ_{Total} , is given by the size of the vector $\phi_{\text{UT}} = \mathbf{\Phi}_1 \oplus \mathbf{\Phi}_2 \oplus \dots \oplus \mathbf{\Phi}_\rho$, and the weight of each iteration is given by $\psi_{\text{UT}} = \mathbf{\Psi}_1 \otimes \mathbf{\Psi}_2 \otimes \dots \otimes \mathbf{\Psi}_\rho$, yielding a new stochastic set, $\mathbf{\Omega}_{\text{UT}} = [\phi_1, \dots, \phi_{\zeta_{\text{Total}}}]$, which outputs a simulation result in each k -th iteration, $\mathbf{f}_k(\mathbf{\Omega}_{\text{UT}}) = \hat{\mathbf{\Lambda}}_k$. The set of all UT iteration results is

$$\mathbf{\Lambda}_{\text{UT}} = [\hat{\mathbf{\Lambda}}_1, \dots, \hat{\mathbf{\Lambda}}_{\zeta_{\text{Total}}}]$$

Hence, the UT simulation can run using an individual Sigma point for each RV such as:

$$\mathbf{F}(\mathbf{\Omega}_{\text{UT}}) = \mathbf{E}[\mathbf{\Lambda}_{\text{UT}}] = \sum_{k=1}^{\zeta_{\text{Total}}} \psi_{\text{UT}}(k) \hat{\mathbf{\Lambda}}_k \quad (4.9)$$

4.3 Computation of the UT

The computation of UT is fairly simple, if the statistical moments of a PDF are known the computation of the Sigma and weight points can be done instantly, if not a mathematical expansion, such the Taylor-Maclaurin expansion, is needed [1, 2, 9, 8, 17, 16].

4.3.1 Finding the statistical moments of an unknown PDF with the Taylor-Maclaurin expansion

In order to proceed to a demonstration of the technique, lets assume two unknown RVs with the same characteristics, being $\mathbf{\Omega}$ a continuous RV and $\hat{\mathbf{\Omega}}$ a discrete RV. The n -th statistical moments are computed in a similar fashion, as stated in (3.9):

$$\begin{aligned} \mathbf{E}[\mathbf{\Omega}^n] &= \mathbf{E}[\hat{\mathbf{\Omega}}^n] \\ \int \mathbf{\Omega}^n p(\mathbf{\Omega}) d\mathbf{\Omega} &= \sum \hat{\mathbf{\Omega}}^n p(\hat{\mathbf{\Omega}}) \end{aligned} \quad (4.10)$$

Since the PDF is unknown, a polynomial expansion is needed, the Taylor-Mclaurin expansion [28, 29, 30, 15] states that a function can be expressed in terms of polynomials, thus:

$$f(\mathbf{\Omega}) = a_0 + a_1 \mathbf{\Omega} + a_2 \mathbf{\Omega}^2 + \dots + a_k \mathbf{\Omega}^k. \quad (4.11)$$

Using Equation (4.10), we have:

$$\mathbf{E}[f(\mathbf{\Omega})] = \mathbf{E}[a_0] + \mathbf{E}[a_1 \mathbf{\Omega}] + \mathbf{E}[a_2 \mathbf{\Omega}^2] + \dots + \mathbf{E}[a_k \mathbf{\Omega}^k], \quad (4.12)$$

given that the coefficients are constants, the expectancy calculus yields:

$$\mathbf{E}[f(\mathbf{\Omega})] = a_0 + a_1 \mathbf{E}[\mathbf{\Omega}] + a_2 \mathbf{E}[\mathbf{\Omega}^2] + \dots + a_k \mathbf{E}[\mathbf{\Omega}^k]. \quad (4.13)$$

With Equation (4.13), it is possible to view that the Taylor expansion provides the pure PDF moments weighted by linear coefficients, so it is possible to use the stochastics concepts to extract the proper stochastic moments from the Taylor polynomial using a finite set $\mathbf{\Omega} = [\mathbf{\Omega}_1, \mathbf{\Omega}_2, \dots, \mathbf{\Omega}_z]$

of variables:

$$\begin{aligned}
\mathbf{E}[\Omega^0] &= \sum \Omega^0 f(\Omega) = f(\Omega_1) + f(\Omega_2) + \cdots + f(\Omega_z), \\
\mathbf{E}[\Omega] &= \sum \Omega f(\Omega) = \Omega(f(\Omega_1) + f(\Omega_2) + \cdots + f(\Omega_z)), \\
\mathbf{E}[\Omega^2] &= \sum \Omega^2 f(\Omega) = \Omega^2(f(\Omega_1) + f(\Omega_2) + \cdots + f(\Omega_z)), \\
&\vdots \\
\mathbf{E}[\Omega^k] &= \sum \Omega^k f(\Omega) = \Omega^k(f(\Omega_1) + f(\Omega_2) + \cdots + f(\Omega_z)).
\end{aligned} \tag{4.14}$$

4.3.2 Choosing the Sigma points and computing the weight points

In order to choose the Sigma points from the RV, Ω , some rules must be strictly adhered to:

1. $\int_{-\infty}^{+\infty} f(\Omega) d\Omega = \sum_{k=-\infty}^{+\infty} p(\Omega_k) = 1$ [13, 12]
2. The Sigma points first must be symmetrical, then properly adjusted, if non-symmetric spacing is necessary [17, 16, 1, 2].
3. The moment calculations according to the Equations (3.9) and (3.10) must always be true [12, 13, 17, 16, 1, 2].
4. The computation of the first statistical moment is mandatory.

It is a good practice to choose a number of Sigma points at least one order higher than the critical statistical moment in the simulation scenario. For example, if in the simulation environment the average is critical, then at least two sigma points are needed (first statistical moment plus one equals two); if the variance is critical, at least three sigma points are needed (second statistical moment plus one equals three).

The Sigma points are symmetrically distributed around the mean value; therefore, to compute a set Φ that contains an even ζ Sigma points, with the statistical moments found according to Subsection 4.3.1, we do as following:

$$\begin{aligned}
\sum_{z=1}^{\zeta} p(\Omega_z) &= 1, \\
\sum_{z=1}^{\zeta} \Omega_z p(\Omega_z) &= \mathbf{E}[\Xi], \\
\sum_{z=1}^{\zeta} \Omega_z^2 p(\Omega_z) &= \mathbf{E}[\Xi^2], \\
&\vdots \\
\sum_{z=1}^{\zeta} \Omega_z^k p(\Omega_z) &= \mathbf{E}[\Omega^k].
\end{aligned} \tag{4.15}$$

A linear system comprised of k variables and k equations is setup, so that $\zeta < k$, is to be solved with the following conditions. If the set $\Phi = [\phi(1), \dots, \phi(\zeta)]$ contains an even number of Sigma points, then the set median does not match a Sigma point, taking that the points around the median have the index close to $\frac{\zeta}{2}$:

$$\begin{aligned}
\mathbf{E}[\Omega] - \phi(1) &= \mathbf{E}[\Omega] + \phi(\zeta) \implies \psi(1) = \psi(\zeta), \\
\mathbf{E}[\Omega] - \phi(2) &= \mathbf{E}[\Omega] + \phi(\zeta - 1) \implies \psi(2) = \psi(\zeta - 1), \\
\mathbf{E}[\Omega] - \phi(3) &= \mathbf{E}[\Omega] + \phi(\zeta - 2) \implies \psi(3) = \psi(\zeta - 2), \\
&\vdots \\
\mathbf{E}[\Omega] - \phi(z) &= \mathbf{E}[\Omega] + \phi(\zeta - z - 1) \implies \psi(z) = \psi(\zeta - z - 1).
\end{aligned} \tag{4.16}$$

Given that the weight points are the probability of the Sigma points, as stated in Section 4.2, $p(\Phi) = \Psi = [\psi(1), \dots, \psi(\zeta)]$. Applying the first rule presented in this subsection, we obtain:

$$2 \sum_{z=1}^{\frac{\zeta}{2}} \psi(z) = 1. \tag{4.17}$$

If the set contains an odd number of points, then the median index of the set is $\frac{\zeta+1}{2}$ and it matches a Sigma point, that matches the PDF expected value itself:

$$\begin{aligned}
\mathbf{E}[\mathbf{\Omega}] - \phi(1) &= \mathbf{E}[\mathbf{\Omega}] + \phi(\zeta) \implies \psi(1) = \psi(\zeta), \\
\mathbf{E}[\mathbf{\Omega}] - \phi(2) &= \mathbf{E}[\mathbf{\Omega}] + \phi(\zeta - 1) \implies \psi(2) = \psi(\zeta - 1), \\
\mathbf{E}[\mathbf{\Omega}] - \phi(3) &= \mathbf{E}[\mathbf{\Omega}] + \phi(\zeta - 2) \implies \psi(3) = \psi(\zeta - 2), \\
&\vdots \\
\phi\left(\frac{\zeta + 1}{2}\right) &= \mathbf{E}[\mathbf{\Omega}] \implies \psi\left(\frac{\zeta + 1}{2}\right) = \psi\left(\frac{\zeta + 1}{2}\right), \tag{4.18} \\
&\vdots
\end{aligned}$$

$$\mathbf{E}[\mathbf{\Omega}] - \phi(z) = \mathbf{E}[\mathbf{\Omega}] + \phi(\zeta - z - 1) \implies \psi(z) = \psi(\zeta - z - 1). \tag{4.19}$$

Then:

$$\psi\left(\frac{\zeta + 1}{2}\right) + 2 \sum_{z=1}^{\frac{\zeta-1}{2}} \psi(z) = 1. \tag{4.20}$$

Note that Equations (4.16) and (4.19) are the same, except that one must consider Equation (4.18) if the set has an odd number of points.

4.3.3 Computation of the UT for the unitary variance, zero-mean, Gaussian Distribution

In the scope of this work, the Gaussian PDF is of great importance, thus it is interesting to illustrate how the UT is computed for it.

The Gaussian PDF is well known and is commonly applied throughout engineering and other fields. Its moments are already calculated [12, 13, 14], as shown in Table 4.1:

Table 4.1: Zero-mean, Gaussian PDF statistical moments [12, 13, 14].

Moment Order	Value
1	0
2	σ^2
3	0
4	$3\sigma^4$
5	0
6	$15\sigma^6$
7	0
8	$105\sigma^8$

Using the technique exposed in Subsection 4.3.2, the computation of a three and four-point UT are explained in Subsections (4.3.3.1) and (4.3.3.2), respectively.

4.3.3.1 Three-point UT

- Using Equations 4.20 and 4.15:

$$\psi(2) + 2\psi(1) = 1.$$

$$\phi(1)\psi(1) + \phi(2)\psi(2) + \phi(3)\psi(3) = 0,$$

$$\phi(1)^2\psi(1) + \phi(2)^2\psi(2) + \phi(3)^2\psi(3) = \sigma^2,$$

$$\phi(1)^3\psi(1) + \phi(2)^3\psi(2) + \phi(3)^3\psi(3) = 0,$$

$$\phi(1)^4\psi(1) + \phi(2)^4\psi(2) + \phi(3)^4\psi(3) = 3\sigma^4.$$

- Simplify using Equations 4.18 and 4.19:

$$\phi(2) = 0,$$

$$-\phi(1) = \phi(2),$$

$$2\phi(1)^2\psi(1) = \sigma^2,$$

$$2\phi(1)^4\psi(1) = 3\sigma^4.$$

Solving the linear system:

$$\phi(1) = -\sigma\sqrt{3},$$

$$\phi(2) = 0,$$

$$\phi(3) = \sigma\sqrt{3},$$

$$\psi(1) = \frac{1}{6},$$

$$\psi(2) = \frac{2}{3},$$

$$\psi(3) = \frac{1}{6}.$$

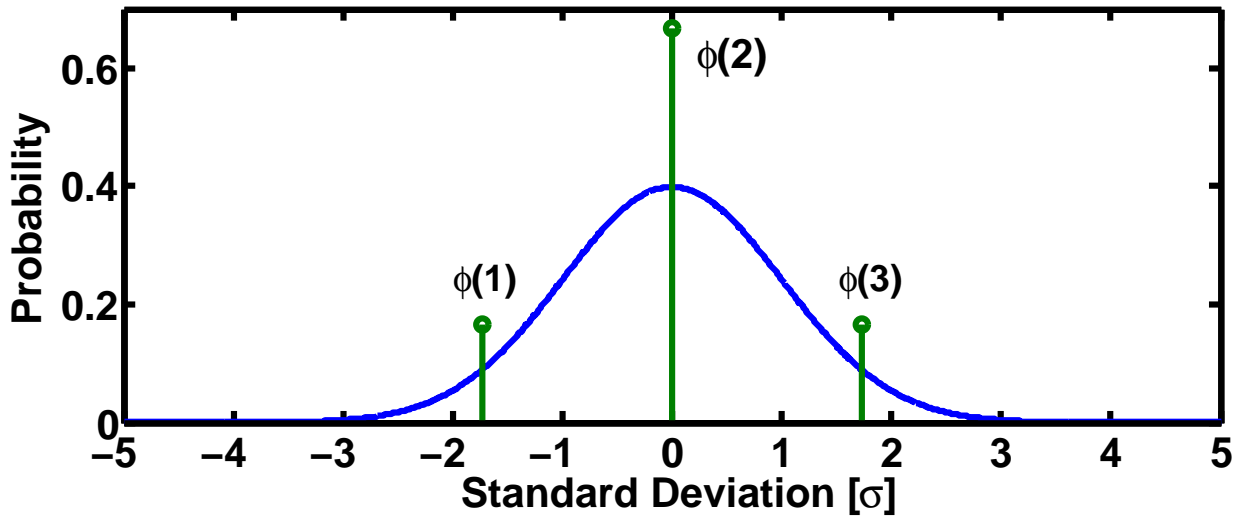


Figure 4.1: 3-point UT vs Gaussian PDF.

4.3.3.2 Four-point UT

- Using Equations 4.17 and 4.15:

$$2\psi(1) + 2\psi(2) = 1.$$

$$\begin{aligned} \phi(1)\psi(1) + \phi(2)\psi(2) + \phi(3)\psi(3) + \phi(4)\psi(4) &= 0, \\ \phi(1)^2\psi(1) + \phi(2)^2\psi(2) + \phi(3)^2\psi(3) + \phi(4)^2\psi(4) &= \sigma^2, \\ \phi(1)^3\psi(1) + \phi(2)^3\psi(2) + \phi(3)^3\psi(3) + \phi(4)^3\psi(4) &= 0, \\ \phi(1)^4\psi(1) + \phi(2)^4\psi(2) + \phi(3)^4\psi(3) + \phi(4)^4\psi(4) &= 3\sigma^4, \\ \phi(1)^5\psi(1) + \phi(2)^5\psi(2) + \phi(3)^5\psi(3) + \phi(4)^5\psi(4) &= 0, \\ \phi(1)^6\psi(1) + \phi(2)^6\psi(2) + \phi(3)^6\psi(3) + \phi(4)^6\psi(4) &= 15\sigma^6. \end{aligned}$$

- Simplify using Equation 4.16:

$$\begin{aligned} -\phi(1) &= \phi(4), \\ -\phi(2) &= \phi(3), \\ 2\phi(1)^2\psi(1) + 2\phi(2)^2\psi(2) &= \sigma^2, \\ 2\phi(1)^4\psi(1) + 2\phi(2)^4\psi(2) &= 3\sigma^4, \\ 2\phi(1)^6\psi(1) + 2\phi(2)^6\psi(2) &= 15\sigma^6. \end{aligned}$$

Solving the linear system:

$$\begin{aligned}
\phi(1) &= -\sigma\sqrt{6 + \sqrt{3}}, & \psi(1) &= \frac{3 - \sqrt{6}}{12}, \\
\phi(2) &= -\sigma\sqrt{6 - \sqrt{3}}, & \psi(2) &= \frac{3 + \sqrt{6}}{12}, \\
\phi(3) &= \sigma\sqrt{6 - \sqrt{3}}, & \psi(3) &= \frac{3 + \sqrt{6}}{12}, \\
\phi(4) &= \sigma\sqrt{6 + \sqrt{3}}. & \psi(4) &= \frac{3 - \sqrt{6}}{12}.
\end{aligned}$$

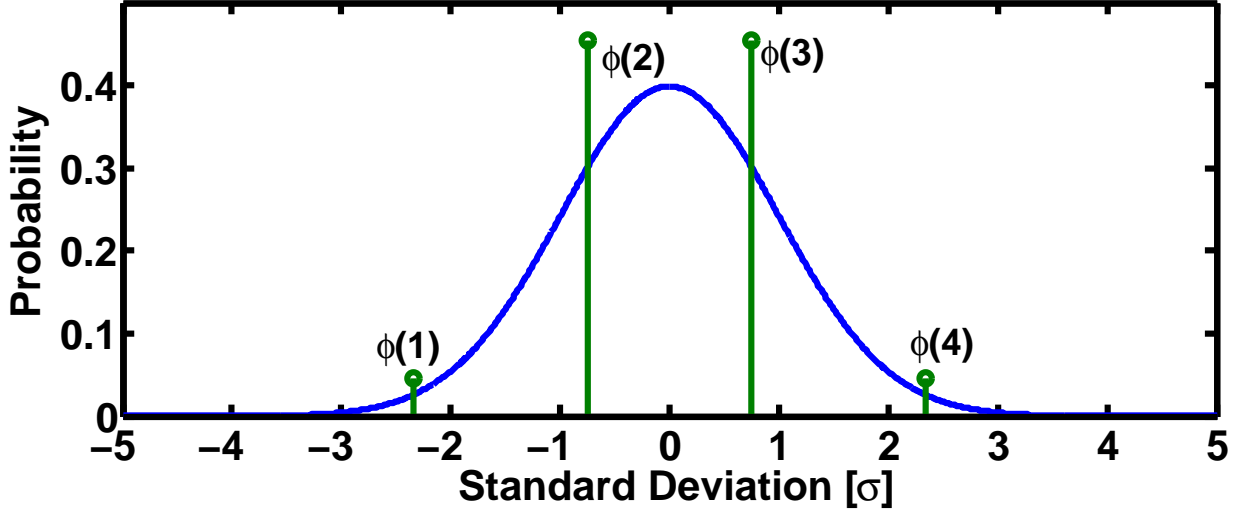


Figure 4.2: 4-point UT vs Gaussian PDF.

4.4 UT convergence vs Monte Carlo convergence

Figures 4.3 and 4.4 show the convergence of a unity mean and variance Gaussian RV, using the techniques of Monte Carlo and UT. A 4-point UT is used and the convergence for the UT is achieved at the fourth iteration for both cases, whilst the Monte Carlo takes at least 1000 iterations before the convergence starts to occur.

For the Monte Carlo simulation, a pseudo-random Gaussian number generator was set to output 100 thousands values. The expected value at the k -th iteration, illustrated in Figure 4.3, is computed by $\mathbf{E}[\Omega]_k = \sum_{z=1}^k \Omega_z p(\Omega_z)$. The variance at the k -th iteration, illustrated in Figure 4.4, is computed by $\mathbf{E}[\Omega^2]_k = \sum_{z=1}^k \Omega_z^2 p(\Omega_z)$.

For the UT simulation, the expected value up to the 4th iteration, illustrated in Figure 4.3, is computed by $\mathbf{E}[\Omega_{\text{UT}}]_k = \sum_{z=1}^4 \phi(z)\psi(z)$. And the variance up to the 4th iteration, illustrated in Figure 4.4, is computed by $\mathbf{E}[\Omega_{\text{UT}}^2]_k = \sum_{z=1}^4 \phi^2(z)\psi(z)$. The UT only needs four iterations to converge, the values from the iteration number 5 to 10^5 are kept only for comparison purposes.

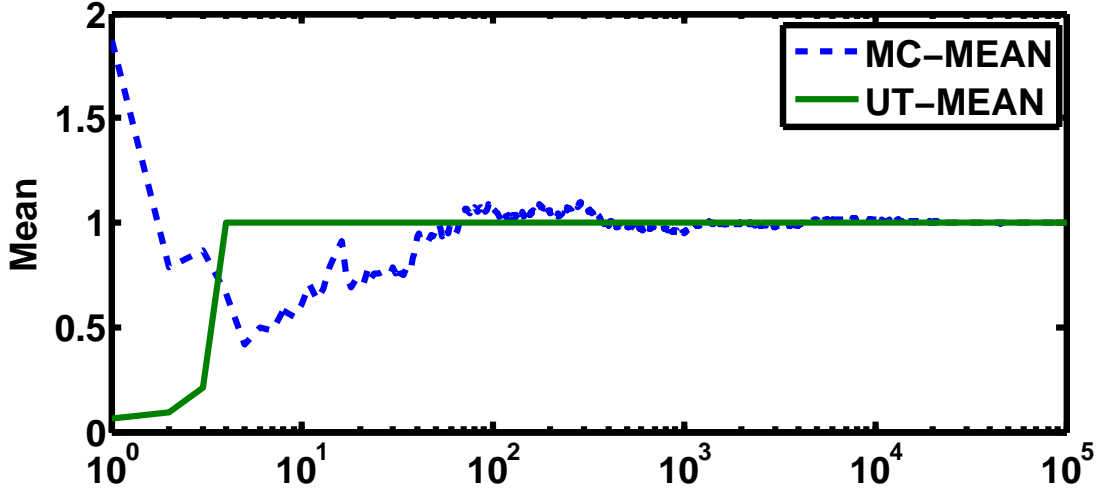


Figure 4.3: Convergence of Monte Carlo and the UT expectancies.

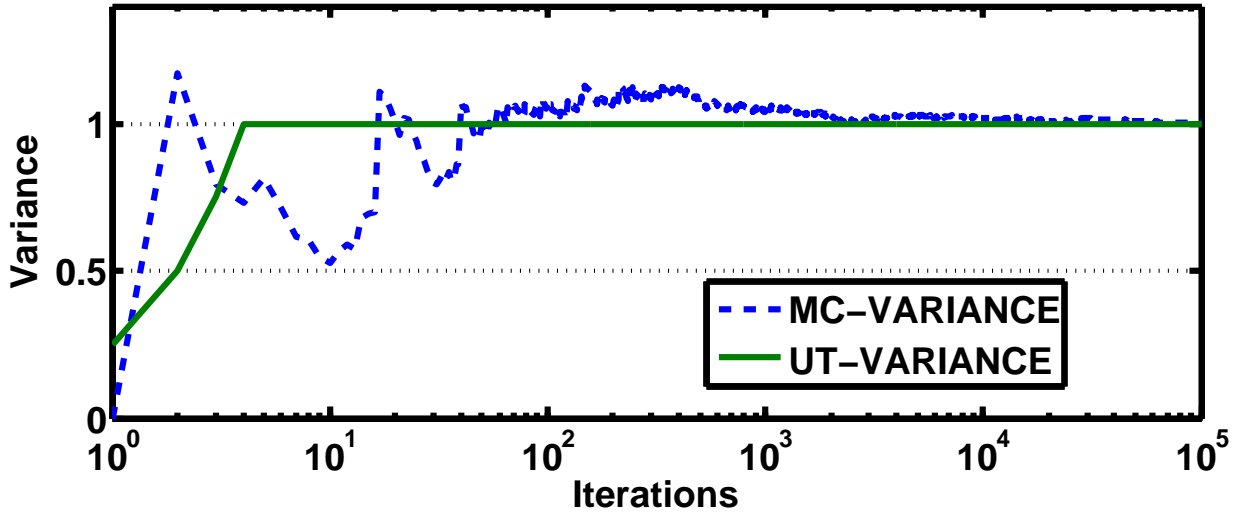


Figure 4.4: Convergence of Monte Carlo and the UT variances.

4.5 Applying the UT for simulations

As shown in Section 3.5, our system output is defined by (3.23). The probabilistic set, Ω , is comprised of \mathbf{S} , which is a BPSK signal, zero-mean discrete Uniform PDF RV, with variance, $\sigma_{\mathbf{S}}^2$, and the complex AWGN, \mathbf{N} , a Gaussian PDF RV with zero-mean and $\sigma_{\mathbf{N}}^2$ variance. Note that the adaptive vector \mathbf{w} depends on the RVs present in the system. We assume that $\mathbf{E}[(\mathbf{A}\mathbf{S})\mathbf{N}] = 0$ and $\mathbf{E}[\mathbf{S}\mathbf{N}] = 0$ [6, 3] and our goal is to find expressions of performance assessment for the signal-to-interference ratio (SIR) and signal-to-interference plus noise (SINR), which are defined as follows:

$$\mathbf{SIR}_{\text{global}} = 10\log_{10} \left(\frac{\sigma_{\mathbf{S},\text{SOI}}^2}{\sum \sigma_{\mathbf{S},\text{INT}}^2} \right) [\text{dB}], \quad (4.21)$$

and

$$\mathbf{SINR}_{\text{global}} = 10 \log_{10} \left(\frac{\sigma_{\mathbf{S},\text{SOI}}^2}{\sum \sigma_{\mathbf{S},\text{INT}}^2 + \sigma_{\mathbf{N}}^2} \right) [\text{dB}]. \quad (4.22)$$

After filtering, the SINR for each sample is calculated using the formula below [19, 9, 8]:

$$\mathbf{f}_n(\boldsymbol{\Omega}) = \mathbf{SINR}(n) = 10 \log_{10} \left(\frac{\mathbf{w}(n) \hat{\mathbf{R}}_{\mathbf{xx}}(n) \mathbf{w}(n)^{\text{H}}}{\mathbf{w}(n) \hat{\mathbf{R}}_{\text{INT+N}}(n) \mathbf{w}(n)^{\text{H}}} \right) [\text{dB}], \quad (4.23)$$

where $\mathbf{R}_{\text{INT+N}}$ is the interference signals plus noise auto-correlation matrix.

Using (4.4), each sample's SINR is given by:

$$\mathbf{F}_n(\boldsymbol{\Omega}) = \mathbf{SINR}_{\text{MC}}(n) = \frac{1}{i} \sum_{k=1}^i \mathbf{SINR}_{\text{MC},k}(n). \quad (4.24)$$

By applying the UT according to the Subsection 4.1, we obtain a the probabilistic $\boldsymbol{\Omega}$ set with two discrete PDFs, a $\zeta_{\mathbf{S}}$ -point discrete Uniform PDF, $\boldsymbol{\Phi}_{\mathbf{S}}$, and a $\zeta_{\mathbf{N}}$ -point PDF, $\boldsymbol{\Phi}_{\mathbf{N}}$, obtained from a continuous Gaussian PDF. Since \mathbf{S} is a BPSK signal, it can be either bit₀ or bit₁, thereby, the two weight points are $\psi_{\mathbf{S},0} = \psi_{\mathbf{S},1} = \frac{1}{2}$, and the two Sigma points are the signal variance $\phi_{\mathbf{S},0} = -\sigma_{\mathbf{S}}$ and $\phi_{\mathbf{S},1} = \sigma_{\mathbf{S}}$. With respect to the noise RV, the $\boldsymbol{\Phi}_{\mathbf{N}}$ and $\boldsymbol{\Psi}_{\mathbf{N}}$ are given by:

$$\boldsymbol{\Phi}_{N_{\mathbb{R}}} = [\phi_{\mathbf{N},1}, \phi_{\mathbf{N},2}, \dots, \phi_{\mathbf{N},\zeta_{\mathbf{N}}}], \quad (4.25)$$

$$\boldsymbol{\Phi}_{N_{\mathbb{Q}}} = [\phi_{\mathbf{N},1}, \phi_{\mathbf{N},2}, \dots, \phi_{\mathbf{N},\zeta_{\mathbf{N}}}], \quad (4.26)$$

$$\boldsymbol{\Psi}_{N_{\mathbb{R}}} = [\psi_{\mathbf{N},1}, \psi_{\mathbf{N},2}, \dots, \psi_{\mathbf{N},\zeta_{\mathbf{N}}}], \quad (4.27)$$

$$\boldsymbol{\Psi}_{N_{\mathbb{Q}}} = [\psi_{\mathbf{N},1}, \psi_{\mathbf{N},2}, \dots, \psi_{\mathbf{N},\zeta_{\mathbf{N}}}], \quad (4.28)$$

In order to cover all possible noise combinations, we perform the Kronecker sum of two vectors defined in (3.8):

$$\boldsymbol{\Phi}_{\mathbf{N},\mathbb{C}} = \text{dediag}(\boldsymbol{\Phi}_{N_{\mathbb{R}}} \oplus j \boldsymbol{\Phi}_{N_{\mathbb{Q}}}). \quad (4.29)$$

and the weight points set is, resulting in a total of $\zeta_{\mathbf{N}}^2$ combinations:

$$\boldsymbol{\Psi}_{N_{\mathbb{C}}} = \boldsymbol{\Psi}_{N_{\mathbb{R}}} \cap \boldsymbol{\Psi}_{N_{\mathbb{Q}}} = \boldsymbol{\Psi}_{N_{\mathbb{R}}} \otimes \boldsymbol{\Psi}_{N_{\mathbb{Q}}}. \quad (4.30)$$

As the noise is uncorrelated to the signal, then:

$$\begin{aligned} \mathbf{p}(\boldsymbol{\Omega}) &= [\boldsymbol{\Psi}_{\mathbf{S}} \cap \boldsymbol{\Psi}_{N_{\mathbb{C}}}] = [\boldsymbol{\Psi}_{\mathbf{S},0} \cap \boldsymbol{\Psi}_{N_{\mathbb{C}}}] \cup [\boldsymbol{\Psi}_{\mathbf{S},1} \cap \boldsymbol{\Psi}_{N_{\mathbb{C}}}], \\ \boldsymbol{\Psi}_{\text{UT}} &= [\psi_{\text{UT},1}, \psi_{\text{UT},2}, \dots, \psi_{\text{UT},2\zeta_{\mathbf{N}}}], \end{aligned} \quad (4.31)$$

which is the same as computing $\Psi_{\mathbf{N}_c} \otimes \Psi_{\mathbf{S}}$, yielding a $2\zeta_{\mathbf{N}} = \zeta_{\mathbf{S}}\zeta_{\mathbf{N}}$ -iteration UT simulation.

Using (3.22) presented in Section 3.5, the whole adaptive system is simulated in the $2\zeta_{\mathbf{N}}$ -iteration UT simulation, using the BPSK bit_0 at the first $\zeta_{\mathbf{N}}$ iterations, then BPSK bit_1 at the last $\zeta_{\mathbf{N}}$ iterations:

$$[\hat{\mathbf{X}}_k = \mathbf{a}(\theta_0)\phi_{\mathbf{S},0} + \mathbf{A}_{\text{int}}\phi_{\mathbf{S},0} + \Phi_{\mathbf{N}_c,k}]_{k=1}^{\zeta_{\mathbf{N}}} \quad (4.32)$$

$$[\hat{\mathbf{X}}_k = \mathbf{a}(\theta_0)\phi_{\mathbf{S},0} + \mathbf{A}_{\text{int}}\phi_{\mathbf{S},1} + \Phi_{\mathbf{N}_c,k}]_{k=1}^{\zeta_{\mathbf{N}}}. \quad (4.33)$$

Since the interferers suffer spatial multiplexing and, for the sake of simplicity, their variances are known and are assumed to be uncorrelated to the SOI. According to our simulations, the influence of including the combinations between SOI and interferers is negligible due to the LCMV filtering. However, in a more complex system, these combinations must be taken into account.

Using (4.9):

$$\mathbf{F}_n(\Omega) = \mathbf{SINR}_{\text{UT}}(n) = \sum_{k=1}^{2\zeta_{\mathbf{N}}} \psi_{\text{UT},k} \mathbf{SINR}_{\text{UT},k}(n) \quad (4.34)$$

For the UT simulations, using the concepts of Subsection 3.3, a Taylor expansion satisfying (3.10) was performed on the AWGN PDF in order to obtain four Sigma and weight points, and two Sigma points were obtained for the BPSK signal discrete Uniform PDF, which are presented in Table 4.2.

Table 4.2: Calculated UT Sigma and weight points for the Gaussian noise ($\Phi_{\mathbf{N}}, \Psi_{\mathbf{N}}$) and the BPSK signal ($\Phi_{\mathbf{S}}, \Psi_{\mathbf{S}}$).

$\Phi_{\mathbf{N}}$	Value	$\Psi_{\mathbf{N}}$	Value
$\phi_{\mathbf{N},1}$	$-\sigma_{\mathbf{N}}\sqrt{6 + \sqrt{3}}$	$\psi_{\mathbf{N},1}$	$\frac{3-\sqrt{6}}{12}$
$\phi_{\mathbf{N},2}$	$-\sigma_{\mathbf{N}}\sqrt{6 - \sqrt{3}}$	$\psi_{\mathbf{N},2}$	$\frac{3+\sqrt{6}}{12}$
$\phi_{\mathbf{N},3}$	$\sigma_{\mathbf{N}}\sqrt{6 - \sqrt{3}}$	$\psi_{\mathbf{N},3}$	$\frac{3+\sqrt{6}}{12}$
$\phi_{\mathbf{N},4}$	$\sigma_{\mathbf{N}}\sqrt{6 + \sqrt{3}}$	$\psi_{\mathbf{N},4}$	$\frac{3-\sqrt{6}}{12}$
$\Phi_{\mathbf{S}}$	Value	$\Psi_{\mathbf{S}}$	Value
$\phi_{\mathbf{S},0}$	-1	$\psi_{\mathbf{S},0}$	$\frac{1}{2}$
$\phi_{\mathbf{S},1}$	1	$\psi_{\mathbf{S},1}$	$\frac{1}{2}$

Computing (4.31), according to the Subsections 4.5 and 4.1, we obtain a 32-point UT simulation, resulting in every possible combination between the signals and noises weight points, as shown in Table 4.3.

Table 4.3: Combination of the UT weight points, for each ζ -th iteration.

ζ	Bit 0	ζ	Bit 1
-	$\psi_{\mathbf{S},0} \cap \Psi_{\mathbf{N},\mathbf{C}}$	-	$\psi_{\mathbf{S},1} \cap \Psi_{\mathbf{N},\mathbf{C}}$
1	$0.5(\psi_{\mathbf{N}_R,1})(\psi_{\mathbf{N}_Q,1})$	17	$0.5(\psi_{\mathbf{N}_R,1})(\psi_{\mathbf{N}_Q,1})$
2	$0.5(\psi_{\mathbf{N}_R,1})(\psi_{\mathbf{N}_Q,2})$	18	$0.5(\psi_{\mathbf{N}_R,1})(\psi_{\mathbf{N}_Q,2})$
3	$0.5(\psi_{\mathbf{N}_R,1})(\psi_{\mathbf{N}_Q,3})$	19	$0.5(\psi_{\mathbf{N}_R,1})(\psi_{\mathbf{N}_Q,3})$
4	$0.5(\psi_{\mathbf{N}_R,1})(\psi_{\mathbf{N}_Q,4})$	20	$0.5(\psi_{\mathbf{N}_R,1})(\psi_{\mathbf{N}_Q,4})$
5	$0.5(\psi_{\mathbf{N}_R,2})(\psi_{\mathbf{N}_Q,1})$	21	$0.5(\psi_{\mathbf{N}_R,2})(\psi_{\mathbf{N}_Q,1})$
6	$0.5(\psi_{\mathbf{N}_R,2})(\psi_{\mathbf{N}_Q,2})$	22	$0.5(\psi_{\mathbf{N}_R,2})(\psi_{\mathbf{N}_Q,2})$
7	$0.5(\psi_{\mathbf{N}_R,2})(\psi_{\mathbf{N}_Q,3})$	23	$0.5(\psi_{\mathbf{N}_R,2})(\psi_{\mathbf{N}_Q,3})$
8	$0.5(\psi_{\mathbf{N}_R,2})(\psi_{\mathbf{N}_Q,4})$	24	$0.5(\psi_{\mathbf{N}_R,2})(\psi_{\mathbf{N}_Q,4})$
9	$0.5(\psi_{\mathbf{N}_R,3})(\psi_{\mathbf{N}_Q,1})$	25	$0.5(\psi_{\mathbf{N}_R,3})(\psi_{\mathbf{N}_Q,1})$
10	$0.5(\psi_{\mathbf{N}_R,3})(\psi_{\mathbf{N}_Q,2})$	26	$0.5(\psi_{\mathbf{N}_R,3})(\psi_{\mathbf{N}_Q,2})$
11	$0.5(\psi_{\mathbf{N}_R,3})(\psi_{\mathbf{N}_Q,3})$	27	$0.5(\psi_{\mathbf{N}_R,3})(\psi_{\mathbf{N}_Q,3})$
12	$0.5(\psi_{\mathbf{N}_R,3})(\psi_{\mathbf{N}_Q,4})$	28	$0.5(\psi_{\mathbf{N}_R,3})(\psi_{\mathbf{N}_Q,4})$
13	$0.5(\psi_{\mathbf{N}_R,4})(\psi_{\mathbf{N}_Q,1})$	29	$0.5(\psi_{\mathbf{N}_R,4})(\psi_{\mathbf{N}_Q,1})$
14	$0.5(\psi_{\mathbf{N}_R,4})(\psi_{\mathbf{N}_Q,2})$	30	$0.5(\psi_{\mathbf{N}_R,4})(\psi_{\mathbf{N}_Q,2})$
15	$0.5(\psi_{\mathbf{N}_R,4})(\psi_{\mathbf{N}_Q,3})$	31	$0.5(\psi_{\mathbf{N}_R,4})(\psi_{\mathbf{N}_Q,3})$
16	$0.5(\psi_{\mathbf{N}_R,4})(\psi_{\mathbf{N}_Q,4})$	32	$0.5(\psi_{\mathbf{N}_R,4})(\psi_{\mathbf{N}_Q,4})$

4.6 Numerical Simulations

In order to validate the proposed performance assessment approach, a scenario with a 16 antenna ULA is considered for the full-rank LCMV filter and a 64 antenna ULA with rank reduction to 16 is considered for the reduced-rank LCMV filter, 7 BPSK signals and 2000 snapshots. The DOA of the SOI is 40° while the DOAs of the interfering signals are 20° , 30° , 50° , 60° , 70° and 80° . The SIR is set to -8.45 dB, while the signal-to-noise ratio (SNR) is set to -3 dB. Before filtering, the initial scenario SINR is -9.54 dB.

Each MC iteration results in a SINR based on the noise variance, generated from a continuous Gaussian PDF, and a BPSK bit variance based on a discrete Uniform PDF. The SINR is calculated according to (4.23) and the final results are obtained according to (4.24).

The UT simulation is setup to run the first 16 iterations with the filter being input with values according to (4.32) and the later 16 iterations according to (4.33).

For each iteration, the obtained $\hat{\mathbf{R}}_{\mathbf{X}\mathbf{X}}$ and $\hat{\mathbf{R}}_{\mathbf{I}\mathbf{N}\mathbf{T}+\mathbf{N}}$ are used to calculate the SINR for each sample, according to (4.23) 32 distinct SINR values are obtained, with final SINR, for each sample being calculated as of (4.34).

4.6.1 First Approach

In order to illustrate the different natures of the MC and UT simulations, Figure 4.5 shows the SINR of the SOI. Each solid line is the SINR found for a single UT iteration, without computing the expectancy according to (4.34), while the dots are the SINR given by one MC iteration. Note

that the dots are considerably outspread due to the continuous nature of the Gaussian PDF. Therefore, performing only few MC iterations may result into performance assessment curves that are vastly different from the ones obtained after several MC iterations.

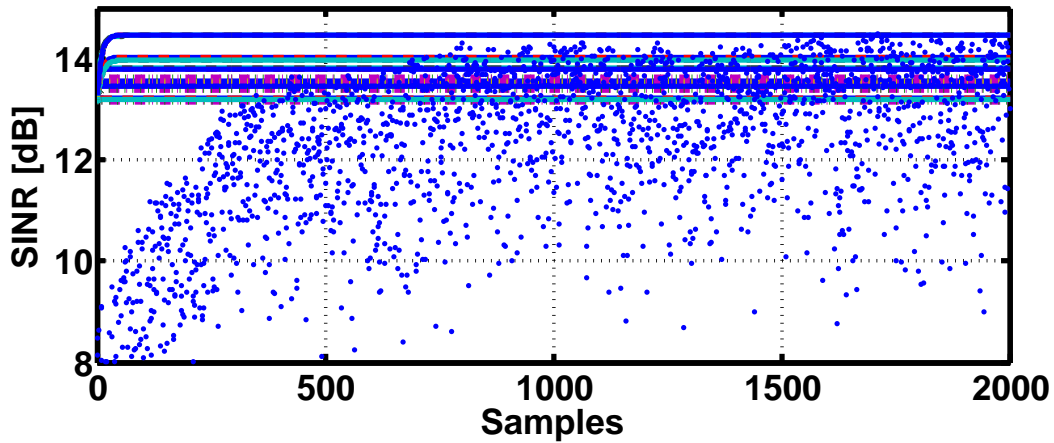


Figure 4.5: SINR (dB) vs sample numbers, before using 4.34 to calculate the final expectancy for UT curves.

4.6.2 Full-rank LCMV simulations

The SINR final results are illustrated in Figures 4.6 and 4.7, with a solid line for MC, after (4.24), and a dashed line for the UT, after (4.34). There is a very slight difference between the results of 0.2 dB. This difference can be reduced by increasing the amount of UT iterations. It is possible to observe the differences of convergence between these Figures, while Figure 4.6 runs 32 MC iterations and presents a low convergence SINR curve for the MC simulation, Figure 4.7 runs 1000 MC iterations and presents a much well behaved SINR MC curve. For both simulation cases, the UT reaches the convergence in 32 iterations.

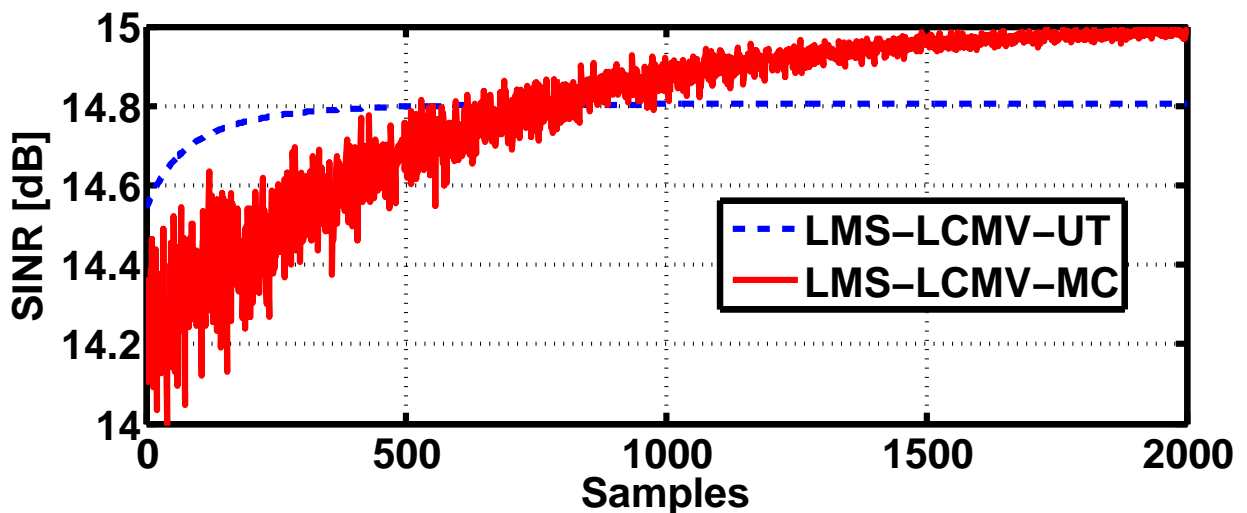


Figure 4.6: SINR (dB) vs sample numbers, 32 Monte Carlo runs, and 32 UT runs.

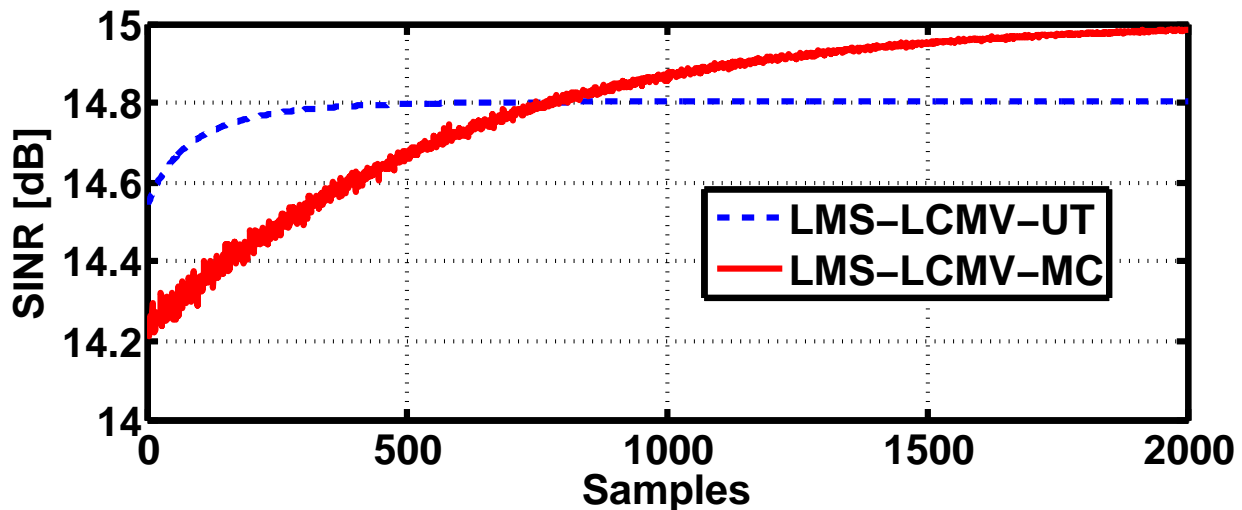


Figure 4.7: SINR (dB) vs sample numbers, 1000 Monte Carlo runs, and 32 UT runs.

Figure 4.8 presents the filter response over the DOAs (beamformer), the highest gain is located at 40° , which is the SOI DOA. The beamformer gain at the SOI DOA is about 85 dB. The MC and UT simulations beamformers are overlapped.

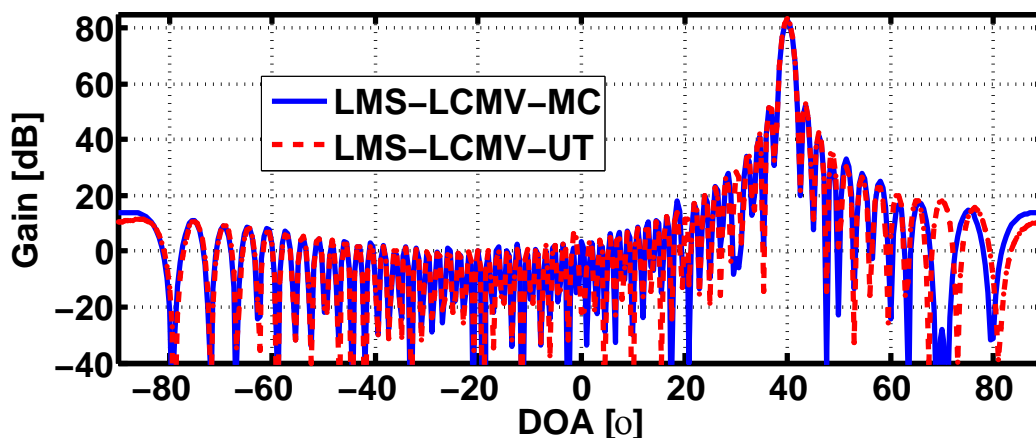


Figure 4.8: Gain (dB) vs DOAs, 1000 Monte Carlo runs and 32 UT runs.

4.6.3 Reduced-rank LCMV simulations

The SINR final results are illustrated in Figures 4.10 and 4.9, with a solid line for MC, after (4.24), and a dashed line for the UT, after (4.34). There is a higher difference between the results of 0.8 dB. There is a higher difference is due to the fact that the reduced rank filter has a computational complexity higher than the full-rank filter, the difference also can be reduced by increasing the amount of UT iterations. As in the previous Subsection, it is possible to observe the differences of convergence between these Figures, while Figure 4.6 runs 32 MC iterations and presents a low convergence SINR curve for the MC simulation, Figure 4.7 runs 1000 MC iterations and presents a much well behaved SINR MC curve. For both simulation cases, the UT reaches the convergence in 32 iterations.

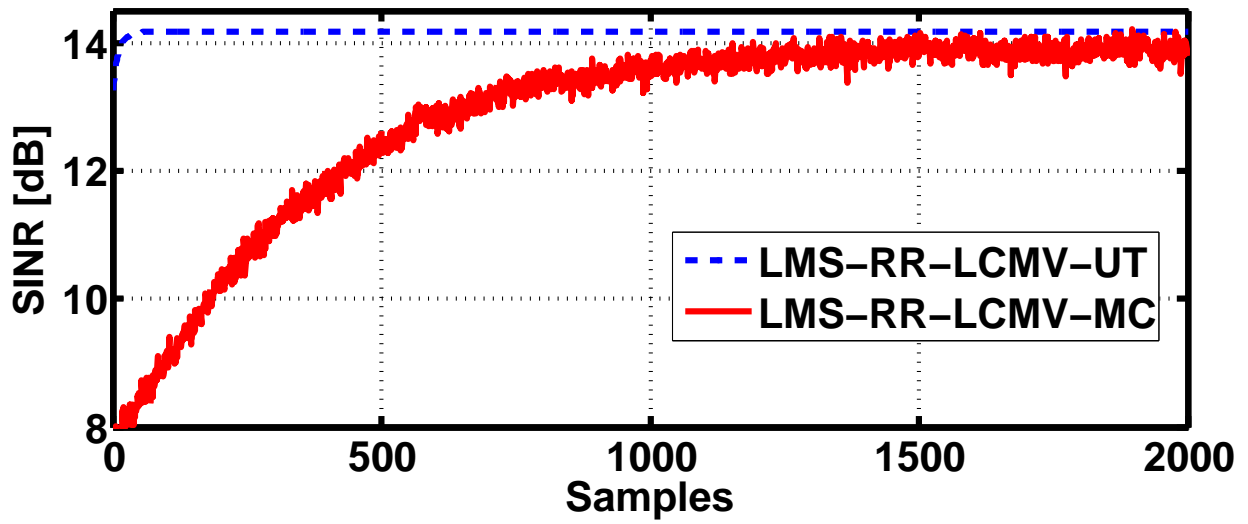


Figure 4.9: SINR (dB) vs sample numbers, 32 Monte Carlo runs, and 32 UT runs.

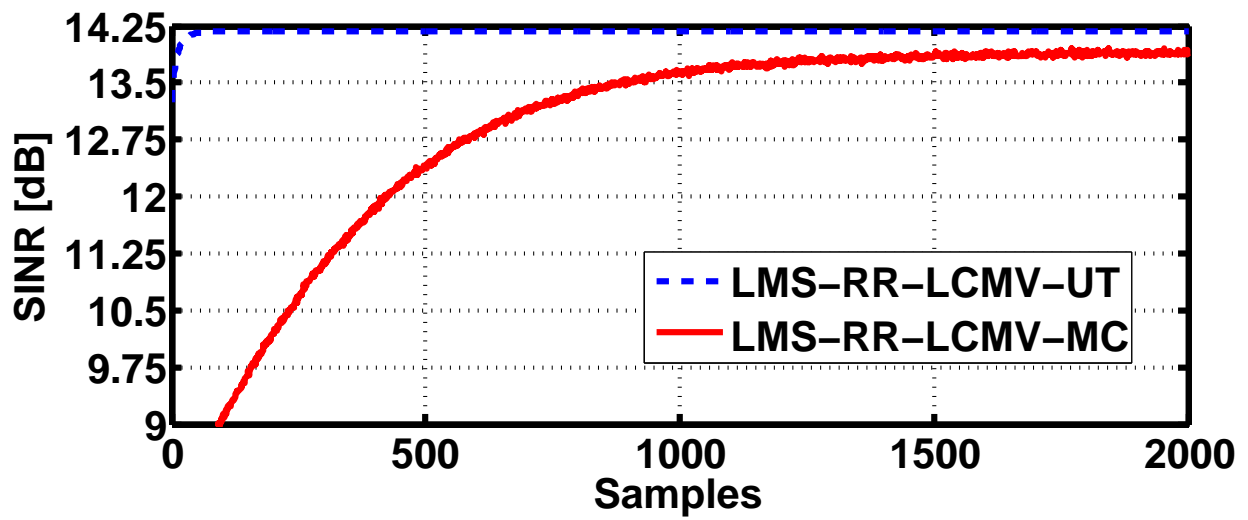


Figure 4.10: SINR (dB) vs sample numbers, 1000 Monte Carlo runs, and 32 UT runs.

Figure 4.11 presents the filter response over the DOAs (beamformer), the highest gain is located at 40° , which is the SOI DOA. The beamformer gain at the SOI DOA is higher than 50 dB. The MC and UT simulations beamformers are overlapped, the UT beamformer lobe is wider due the less complexity in the noise.

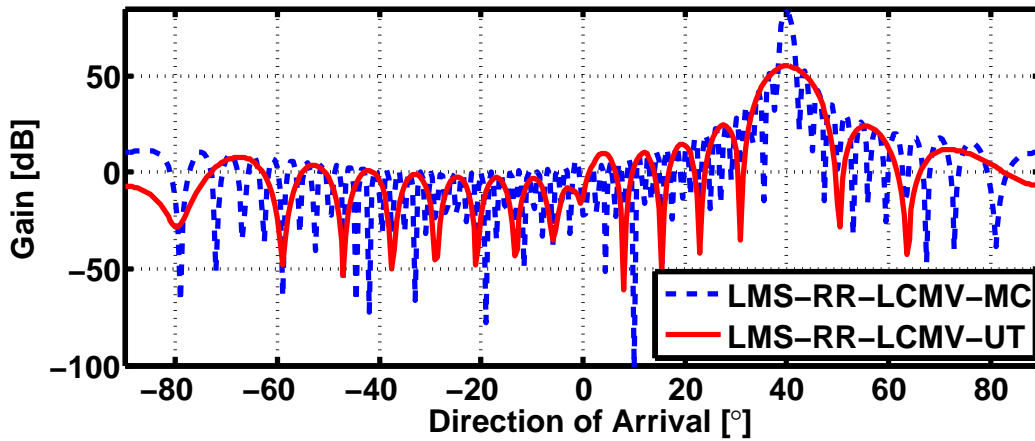


Figure 4.11: Gain (dB) vs DOAs, 1000 Monte Carlo runs and 32 UT runs.

4.6.4 Reduced-rank vs Full-rank LCMV filters

Both UT and MC simulation results are presented in Figures 4.12 and 4.13, respectively, although the UT results hardly differ from that of that MC simulation, as seen in the previous Subsections, making a suitable technique to rapidly evaluate the differences between filtering techniques. The UT clearly shows one of the most important reduced-rank filtering aspects of fast adaption [7, 5, 9, 8], which is difficult to overview in the MC simulation.

The reduced-rank technique has a low SINR loss, about 1 dB, shown by both differences, as a trade-off of the redundancy reduction and faster adaption, the reduced rank filter performed a 64-to-16 dimension reduction, trading off only 1 dB of SINR.

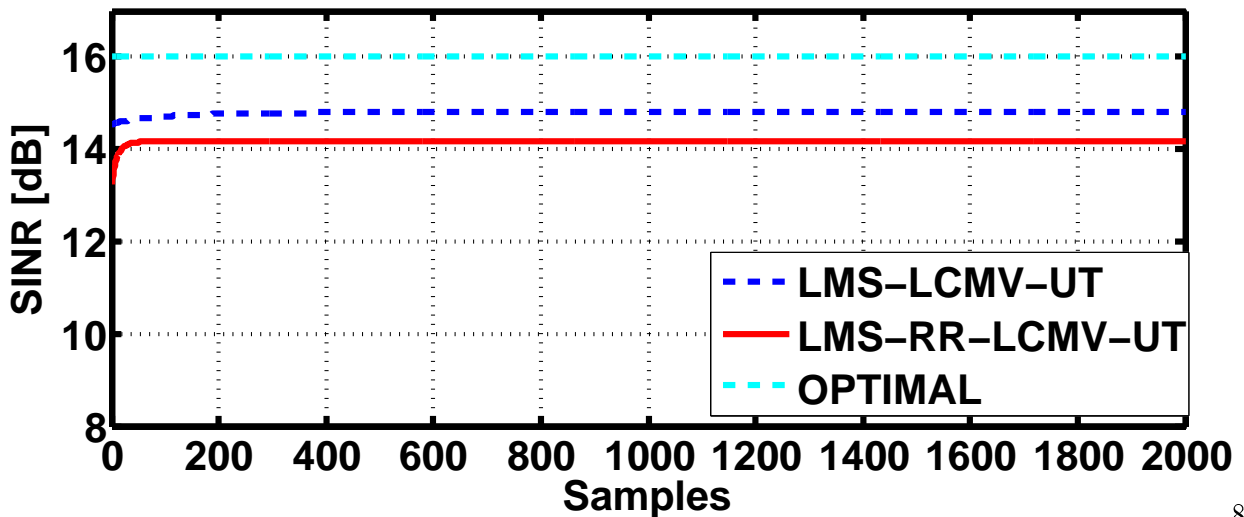


Figure 4.12: SINR (dB) vs sample numbers, for the reduced-rank and full-rank filters, using the UT.

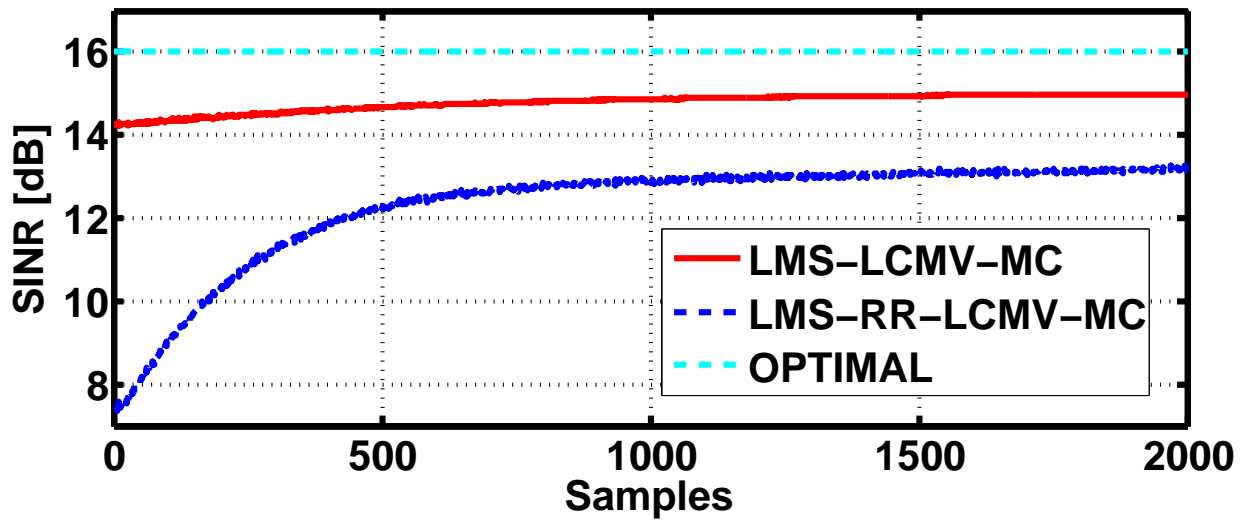


Figure 4.13: SINR (dB) vs sample numbers, for the reduced-rank and full-rank filters, using 1000 MC runs.

Figure 4.14 presents all filters responses over the DOAs (beamformer), using all simulation techniques, the cyan dashed line is the optimum beamformer.

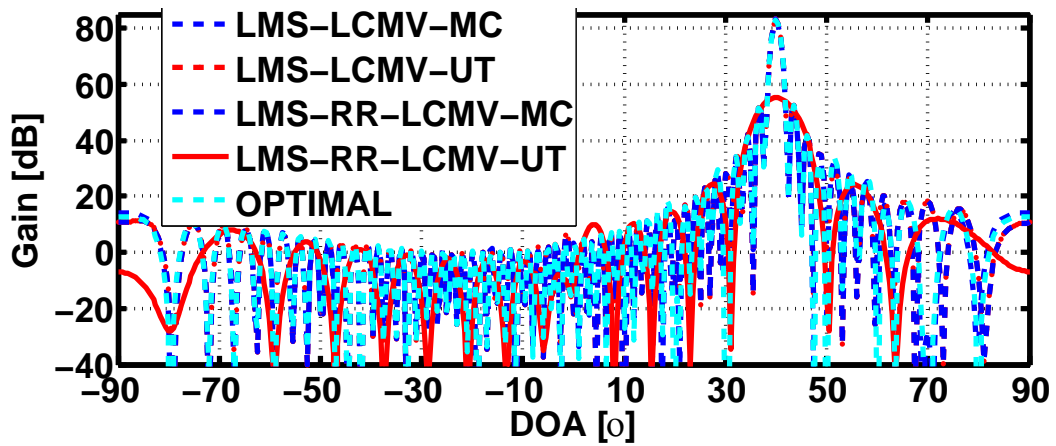


Figure 4.14: All beamformers overlapped.

Chapter 5

Radioaltimeters

Unlike conventional radars, to overcome very low round-trip times at low altitudes, radioaltimeters usually use the frequency modulation continuous wave radars (FM-CW), in which the ranging is done by measuring the beating frequency at the demodulator, which results in a proportionally increasing frequency versus the altitude, caused by the backscattered wave phase-delay [10, 31, 32, 33, 34, 11, 35, 36].

The traditional radioaltimeter, which detects the most powerful backscattered wave, has the advantage to detect the nearest object, in order to alert the airborne systems and pilot to avoid a collision, but has the disadvantage not to detect the actual plane altitude, thus an antenna array solution to model the receiver beamform or to detect the DOA of the backscattered waves is required [10].

This Chapter is divided into three Sections, in which Section 5.1 brings a mathematical explanation of the working principle of the traditional FM-CW radioaltimeter, Section 5.2 introduces and explains the proposed digital antenna array radioaltimeter and Section 5.3 validates the proposed radioaltimeter solution with computer simulations.

5.1 Operational principle of the radioaltimeter

Based on [10, 11], the simplified FM-CW radioaltimeter operational block is illustrated in Figure 5.1. A classic FM-CW radar uses a triangular wave as the modulating signal [10, 32, 36, 35, 31], in order to cancel the Doppler shift caused by the vertical speed or other phenomena [10, 11, 31].

The typical frequencies for the modulating signal falls between 50 Hz and 300 Hz, and the carrier frequency is in the 4.3 GHz frequency band [10, 33, 11], with a ± 100 MHz frequency deviation [10, 36, 35]. Transmitting power ranges from 10 dBm to 27 dBm [10, 11], and the antennas have a directivity around 10 dBi, allowing a wider ground area coverage [11].

To simplify the hardware design, the transmitted signal is generated by a voltage-controlled oscillator (VCO) and it is coupled to the receiver mixer (RF-mixer), acting as the local oscillator (LO) signal. The received backscattered signal is mixed with the LO signal, creating an interme-

mediate frequency (IF) signal, which has the high frequency rejected by the IF low-pass filter (LPF). The IF signal is then amplified through a limiting amplifier and fed to a zero-crossing detector, which is going to generate pulses for a frequency counter, or a digital signal processing device so that the altitude information or some sort of obstacle alarm is triggered [10, 11].

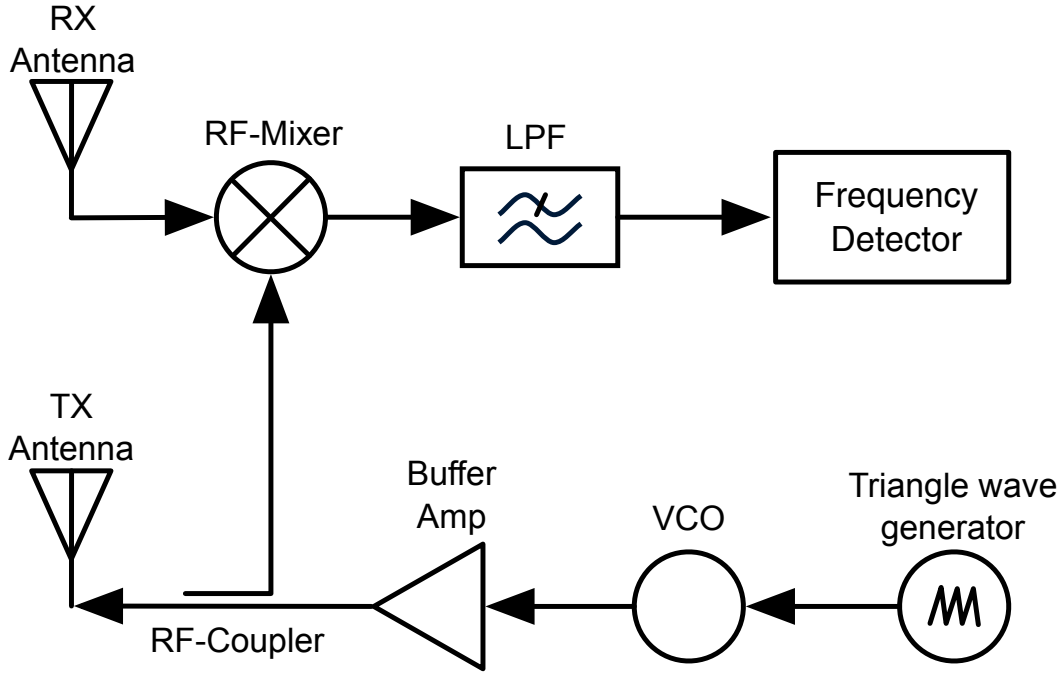


Figure 5.1: Working diagram of a traditional radioaltimeter [10, 11].

5.1.1 Mathematical working principle of the radioaltimeter

The mathematical model of a traditional radioaltimeter is explained by using communication theory concepts [10, 32, 35, 26, 31].

The transmitted signal is generated by a VCO, an electronic oscillator which generates an FM signal according to the input voltage, $v_{in}(t)$, weighted by a gain K_0 in [Hz/V] and $f_0(t)$ as the center frequency[10, 37]:

$$f_{VCO}(t) = f_0 + K_0 \cdot v_{in}(t). \quad (5.1)$$

The instantaneous frequency of an FM signal is given by [26]

$$f_i(t) = f_c + k_f \cdot m(t), \quad (5.2)$$

where f_c is the carrier frequency, k_f is the gain and $m(t)$ is the modulating signal, therefore a VCO generated signal is considered an FM signal [37].

At the VCO input, a triangle waveform $v_{in}(t)$ is used

$$v_{in}(t) = A_0 \cdot m_{triangle}(2\pi f_m t), \quad (5.3)$$

where A_0 and f are the amplitude and signal frequency, respectively. Considering that $f_m = \frac{1}{T}$,

$m_{\text{triangle}}(2\pi f_m t)$ is a triangle waveform, which is a function of t , as illustrated in Figure 5.2.

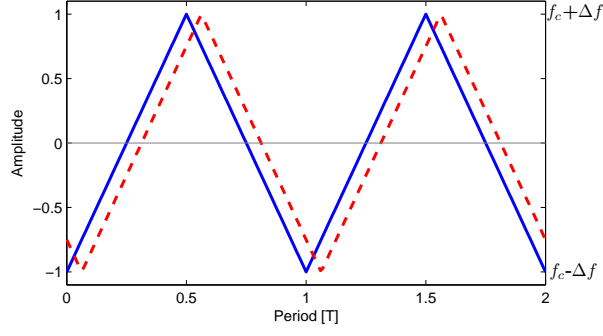


Figure 5.2: Modulating triangle waveform and its phase delayed version. At the positive or negative voltage peaks, the VCO outputs the center frequency, f_c , summed to the positive or negative Δf peak deviations [10].

The triangle wave is periodic. For one period, it is expressed as:

$$m_{\text{triangle}}(t) = \begin{cases} \frac{4t}{T_m} - 1 & \text{for } 0 < t \leq \frac{T_m}{2} \\ \frac{-4t}{T_m} + 3 & \text{for } \frac{T_m}{2} < t \end{cases} . \quad (5.4)$$

By combining (5.2) and (5.3), and considering $k_f \cdot A_0 = \Delta f$ (peak frequency deviation) [10, 26, 32],

$$f_i(t) = f_c + \Delta f \cdot m_{\text{triangle}}(2\pi f_m t), \quad (5.5)$$

the phase term of an FM waveform is [26]

$$\xi(t) = 2\pi \int_0^t f_i(t') dt' = 2\pi(f_c t + \Delta f \int_0^t m_{\text{triangle}}(t') dt), \quad (5.6)$$

The VCO outputs a signal to be transmitted, $t_x(t)$:

$$t_x(t) = \cos(\xi(t)). \quad (5.7)$$

When the signal is backscattered to the receiver, it is attenuated by an α factor and has a time delay, the so-called the round-trip time (rtt):

$$\text{rtt}(r) = \frac{2r}{c}, \quad (5.8)$$

where c is the speed of light and r is the altitude (or the distance).

The received signal is represented by:

$$r_x(t) = \alpha \cdot \cos([\xi(t - \text{rtt})]) = \alpha \cdot t_x(t - \text{rtt}), \quad (5.9)$$

The received signal is mixed, after amplification by a factor of β , for a frequency down-conversion.

The mixing with the local oscillator signal creates an IF signal, which is the so-called beating frequency signal:

$$\text{IF}(t) = \beta\alpha \cdot r_x(t) \cdot t_x(t). \quad (5.10)$$

According to the trigonometric identities, the mixer output $\text{IF}(t)$ contains the sum and difference of frequencies given by

$$\text{IF}(t) = \frac{\beta\alpha}{2}(\cos([\xi(t) + \xi(t - \text{rtt})]) + \cos([\xi(t) - \xi(t - \text{rtt})])), \quad (5.11)$$

where the a high frequency component is suppressed by a low-pass filter located at the mixer output, yielding:

$$\text{IF}'(t) = \frac{\beta\alpha}{2} \cos([\xi(t) - \xi(t - \text{rtt})]). \quad (5.12)$$

The beating frequency from the filtered IF signal is:

$$(5.13)$$

$$= \Delta f \cdot [f_c + \frac{4t}{T_m} - 1 - f_c - \frac{4(t - \text{rtt})}{T_m} + 1] \quad (5.14)$$

$$= \Delta f \cdot (\frac{4\text{rtt}}{T_m}) \quad (5.15)$$

$$f_{\text{IF}'}(\text{rtt}) = 4 \cdot \Delta f \cdot f_m \cdot \text{rtt}. \quad (5.16)$$

Since $\text{rtt}(r) = \frac{2r}{c}$, and (5.16) are linear, the output frequency is a linear function of either the time delay or the altitude. Moreover, the maximum altitude detectable should be less or equal to $\frac{1}{4}$ of $v_{\text{in}}(t)$'s wavelength.

In (5.16), by substituting rtt for (5.8), the detected frequency becomes a function of altitude[32]:

$$f_{\text{altitude}}(r) = \frac{8 \cdot \Delta f \cdot f_m \cdot r}{c}. \quad (5.17)$$

To make the design more compact, leaving space for more antennas, a single-antenna radio altimeter proposed by [34], would be very suitable for an unmanned aerial vehicle (UAV), due to its smaller dimensions and weight. The single antenna proposed in [34] is an FM radio altimeter system that is able to operate in continuous-wave (CW) and interrupted continuous-wave (ICW) modes, and uses a circulator as a duplexer, to separate the transmitted signal from the received signal.

5.2 Proposed digital radioaltimeter

In order to apply digital filters and digital signal processing to the radioaltimeter, a redesign is necessary. Figure 5.3 illustrates the proposed digital radioaltimeter. A triangle wave is digitalized through an analog-to-digital converter (ADC), which will be PSK-modulated and amplified before being transmitted through a single antenna (TX antenna), then the scattered signal is received

by an antenna array (RX ULA), amplified and PSK-demodulated and filtered through a full-rank or reduced-rank LCMV filter, the demodulator and the filter uses the PSK Modulator and ADC output signal as the local oscillator and desired signal references, respectively, the signal is then processed by a digital signal processing processor (DSP processor).

The altitude resolution is related to the signal bandwidth, the higher the bandwidth, the higher the resolution. Since the PSK signal is different, but closely related [27, 26], from an FM or FSK signal it is important to maintain a good triangle wave resolution, therefore, the ADC should run a sampling rate high enough, in order that the low round-trip times causes a significant phase drift, and the bit resolution should be high enough to diminish errors in the metering readings:

$$T_{\text{sample}} = \frac{1}{f_{\text{sample}}} \text{ [s]},$$

$$T_{\text{bit}} = \frac{T_{\text{sample}}}{\text{ADC}_{\text{resolution}}} \text{ [s]}.$$

Where T_{sample} , T_{bit} and f_{sample} are the sampling period, bit period and sampling frequency. To achieve a desired distance resolution, the round-trip time should be observed so that it causes a significant shift in the received stream, using (5.8):

$$T_{\text{bit}} \leq \frac{2r}{c}.$$

For resolutions near one meter:

$$T_{\text{bit}} \leq \frac{2}{3 \cdot 10^8} \leq 6.7 \text{ ns.}$$

$$\text{Bitrate} \geq \frac{1}{T_{\text{bit}}} \geq 150 \text{ Mbps}$$

The differences between the transmitted and the received demodulated signals results in a mean voltage proportional to the altitude, if the aspects presented before are observed, using 5.4:

$$v_{\text{out}}(\text{rtt}) = m_{\text{triangle}}(t) - m_{\text{triangle}}(t - \text{rtt}) \quad (5.18)$$

$$= \begin{cases} \frac{4t}{T_m} - 1 - \frac{4(t-\text{rtt})}{T_m} + 1 & , \forall 0 < t \leq \frac{T_m}{2} \\ \frac{-4t}{T_m} + 3 + \frac{4(t-\text{rtt})}{T_m} - 3 & , \forall 0 < \frac{T_m}{2} < t \end{cases} \quad (5.19)$$

$$= \begin{cases} \frac{4\text{rtt}}{T_m} & , \forall 0 < t \leq \frac{T_m}{2} \\ \frac{4\text{rtt}}{T_m} & , \forall \frac{T_m}{2} < t \end{cases} \quad (5.20)$$

$$v_{\text{out}}(\text{rtt}) = \frac{4\text{rtt}}{T_m} \text{ [V]}. \quad (5.21)$$

Applying (5.8):

$$v_{\text{out}}(\text{rtt}(r)) = \frac{4\text{rtt}(r)}{T_m}, \quad (5.22)$$

$$v_{\text{out}}(r) = \frac{8r}{T_m c}, \quad (5.23)$$

$$v_{\text{out}}(r) = \frac{8r}{\lambda_m} \text{ [V]}. \quad (5.24)$$

Where λ_m is the wavelength of the demodulated signal. Analyzing (5.24) closely, a voltage output of $8 \mu\text{V}/\text{meter}$ is achieved, therefore one of the most important quality of the FM-CW radar is lost: the trade-off between the high bandwidth and the high frequency/m output. To overcome this issue, a high sampling rate of the modulating signal is used, since the sampling frequency must be, at least, twice the sampled signal, according to the Nyquist sampling theorem [26, 27], $v_{\text{out}}(r)$ begins to behave according to the sampling rate:

$$v_{\text{out}}(r, f_{\text{sample}}) = \frac{f_{\text{sample}}}{f_m} \cdot \frac{8r}{\lambda_m}, \quad (5.25)$$

$$v_{\text{out}}(r, f_{\text{sample}}) = \frac{f_{\text{sample}} 8r}{c} \text{ [V]}. \quad (5.26)$$

Thus, if the signal is over-sampled by a sampling frequency a thousand times higher than the modulating frequency, a voltage output of $8 \text{ mV}/\text{meter}$ is achieved, which is a practical voltage to read.

5.3 Simulation scenario setup

In the simulation scenario illustrated in Figure 5.4, three airplanes are flying above different altitudes to the ground, at the same speed and parallel to each other. The main airplane is the one located at the middle. All planes are equipped with the proposed radioaltimeter and the main

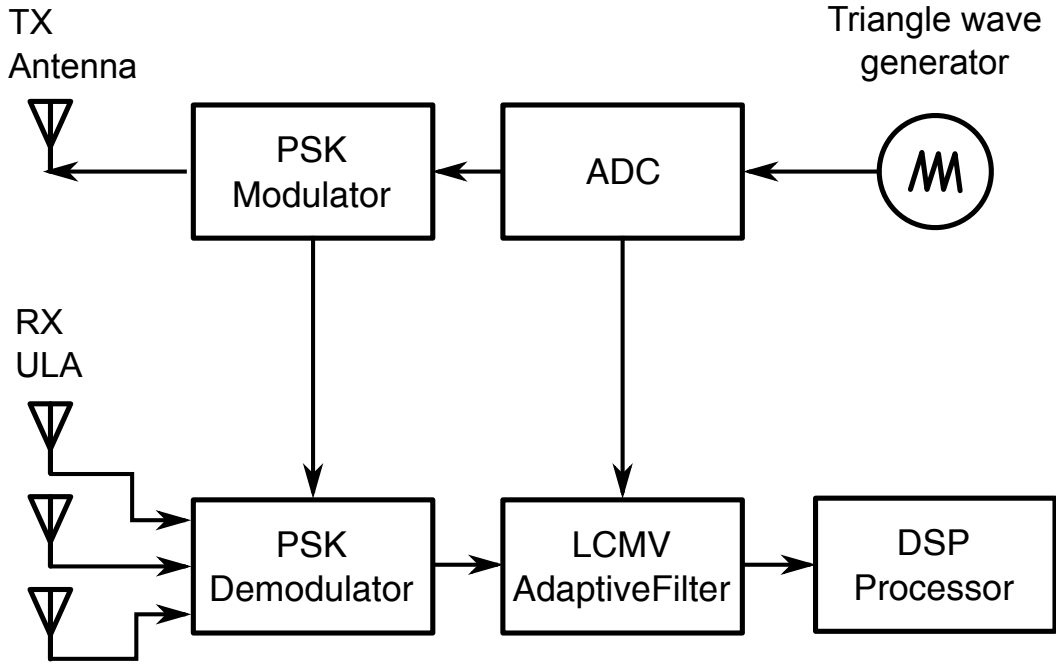


Figure 5.3: Simplified diagram of the proposed radioaltimeter.

plane transmitted signal sequence is known and the line-of-sight (LOS) signal is the SOI, while the known unwanted signals are the non-line-of-sight (NLOS) and the reflections caused by the other planes radars are random and unwanted, considered as interferers (INT).

The main plane altitude, r_{LOS} is set to 100 m above the ground, while the left and right plane altitude is 80 m and 30 m, respectively.

Each plane is spaced by 20 meters and all planes radar cross-sections are set to one square meter, therefore $r_{\text{NLOS}_1} \approx 28.3$ m, $r_{\text{NLOS}_2} \approx 72.8$ m.

The ground is considered to be a perfect reflective surface, thus $r_{\text{INT}_0} = r_{\text{INT}_1} \approx 102.0$ m and the total trip distances for INT_0 and INT_1 are 182 m and 132 m respectively.

The SOI, NLOS_1 , NLOS_2 , INT_0 and INT_1 DOAs' are respectively 0° , 45.30° , -15.95° , 11.36° and -11.36° .

The transmitted power is set to unitary, initial ULA gain is set to 0 dBi as a isotropic irradiator and the whole system is subject to an additive white Gaussian noise, with the SNR varying from 0 dB to -35 dB.

The triangle wave is set to 300 Hz, and the ADC is set to work in a range from 2-bit to 10-bit mode, with the sampling rate at varying from 250 kHz to 25 MHz, in order to output a 2 to 200 Mbps stream. A 200 Mbps requires a bandwidth close to an conventional FM-CW radioaltimeter, and the modem is set to work with a BPSK signal:

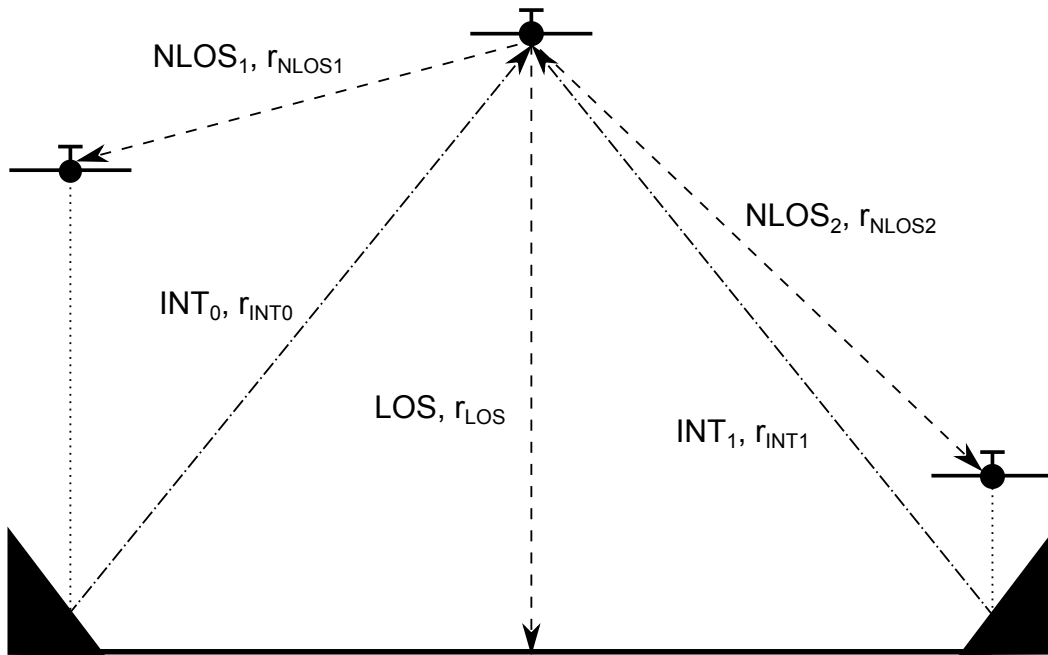


Figure 5.4: Proposed simulation scenario.

5.3.1 Simulation results

Figure (5.5) illustrates how the radioaltimeter behaves in the traditional form, $NLOS_1$ is the highest power component, and it would be the detected distance, for a collision avoidance system it is very useful, but for measuring the actual altitude it is not.

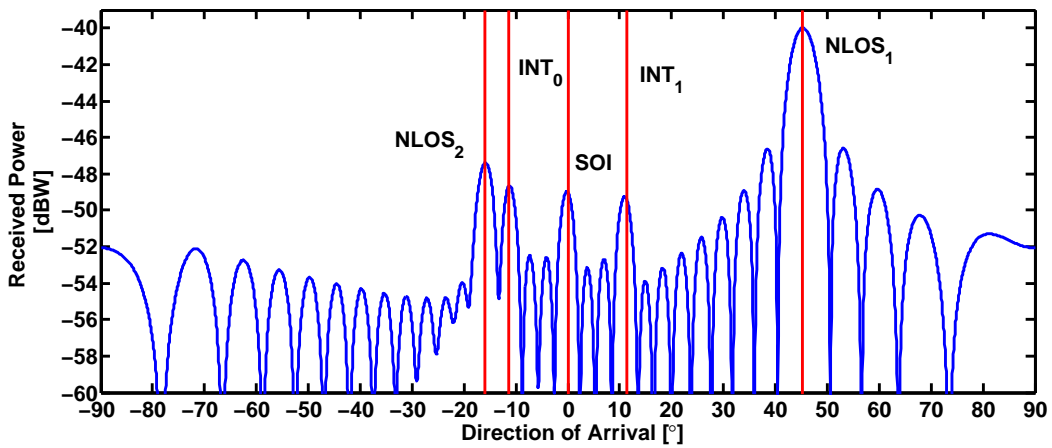


Figure 5.5: Radioaltimeter receiving lobes, before the beamforming.

Figure (5.6) shows the normalized output voltage vs the altitude, for various ADC resolutions at 25 MHz sampling frequency, all lines are overlapped, with little differences. The system shows a linear response over the altitude.

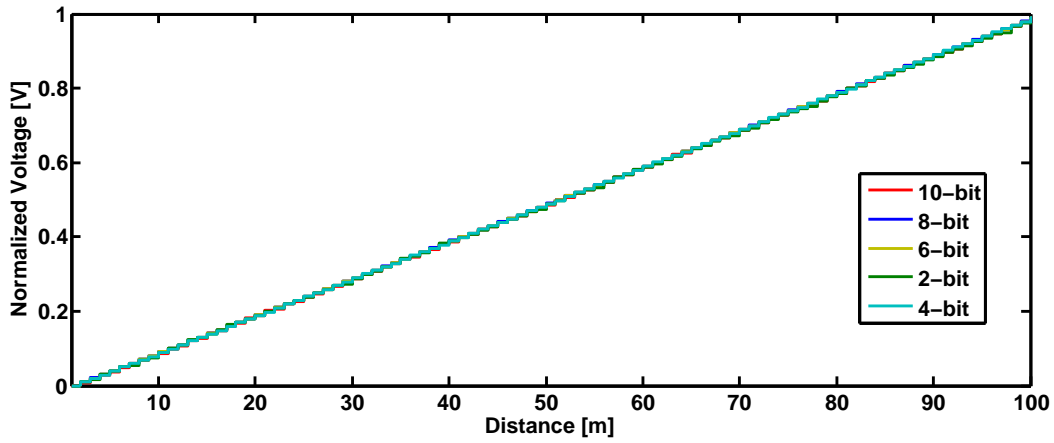


Figure 5.6: Voltage output vs altitude for various ADC resolutions.

Figure (5.7) shows the normalized output voltage vs the altitude, for various ADC sampling rates, at 10-bit resolution, the sampling rate, as stated in Section 5.2, plays a important role in the altitude detection. Only at 25 MHz, when a 200 Mbps bandwidth is reached, the system shows a desirable response.

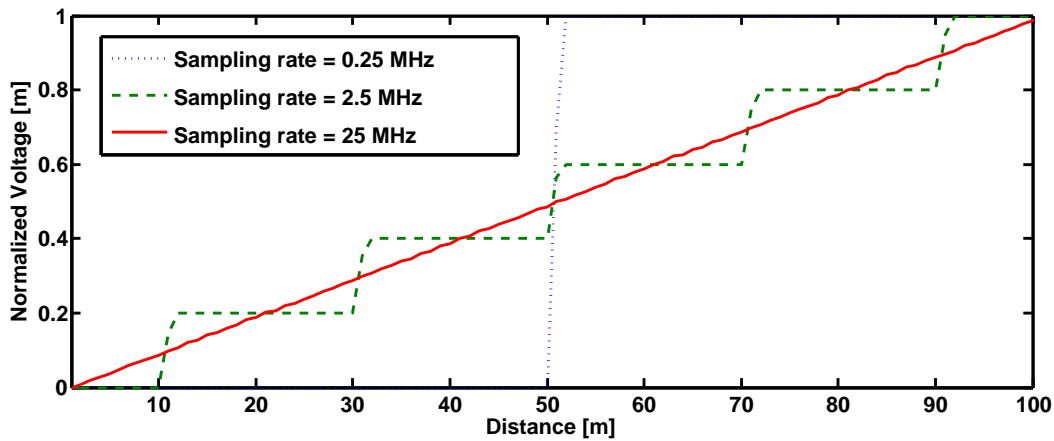


Figure 5.7: Voltage output vs altitude for various ADC sampling rates.

Since radars operates at very low SINR and SNRs, SINR vs samples results, such as the ones shown in Section 4.6, are meaningless. Figure (5.8) shows bit-error-rate (BER) for various SNRs, at -35 dB the systems shows a 10% error, which seems to be high, and indeed is high for data communication, but for altitude detection it is acceptable. In order to improve the BER, the output power or the radar frequency should be raised, in order to raise the radar cross section and the antennas effective aperture. Both UT and MC simulations BER curves overlap.

The reduced-rank adaptive LCMV-BPSK-Radar operates at a 1:2 rank reduction and shows no significant BER raise.

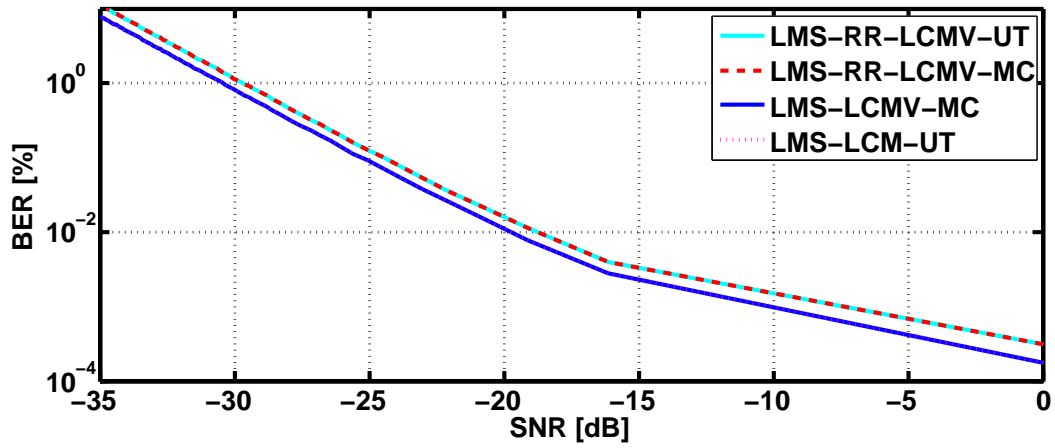


Figure 5.8: Bit-error-rate (BER) for various SNRs, and for the full-rank and reduced rank LCMV-BPSK-Radars

Figure 5.9 shows the antenna beamlobes, after the adaptive LCMV beamforming. The LOS signal is located at 0° and the full-rank LCMV and reduced-rank LCMV beamformers have a 70 dB and 55 dB gain at the SOI DOA. The wider lobe for the reduced-rank case is caused due the rank reduction. Both UT and MC simulations beamlobes overlap.

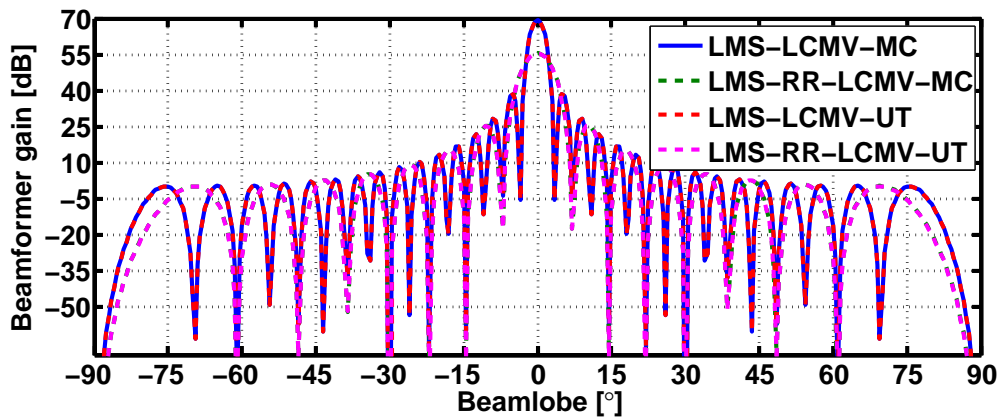


Figure 5.9: Voltage output vs altitude.

Chapter 6

Conclusion

In this work, a UT based low complexity performance assessment technique for adaptive full-rank and reduced-rank LCMV filters has been presented. The proposed UT based performance assessment scheme presents curves with only thirty two UT iterations that closely match curves obtained with one thousand MC iterations.

Even if the UT results not exactly match the Monte Carlo results, it provides a good and reliable preview of such results whilst saving a great amount of time.

The UT improves processing costs and time by discretizing continuous RVs, in our simulations 31.25 times less iterations were needed when using the UT, representing only 5.85% of iterations of MC, which is a huge gain where more complex and dispendious simulations are required. Moreover, the improvements provided by this technique are not solely in the reduction of the number of iterations needed, but, also in the removal of random numbers generators, which further reduces the simulation time and computational requirements, which represented a simulation 41 times faster, computed by the simulating software.

Therefore, the benefits of UT based performance assessment is far reaching, as is not only useful in signal processing applications, but in commercial and industrial applications where the development time should be as short as possible to reduce costs and allow for faster market entry.

The reduced rank filtering technique is very practical and useful in all fields, especially in engineering and geophysics, where sensors arrays are used for all purposes such as radio-frequency signal receiving, structural stress studies, mineral prospection. In such situations, a huge amount of raw data is received, and must be stored for further processing and a fast adaption is needed for communication, surveillance and imaging.

Moreover, this work also proposes a novel digital radioaltimeter or ranging device, which uses a BPSK modulation to range and detect obstacles. Its main contribution is the ability to beamform an ULA with reduced rank and full rank LCMV algorithm in order to fix the ULA gain to a certain direction. The BPSK-LCMV-Radar proposed in this work has a performance of an analog FM-CW radar, with the advantage of beamforming and detecting the real UAV altitude.

OWN PUBLICATIONS

- [1*] R. S. Ferreira Júnior, J. P. C. L. da Costa, R. Nock; R. Zelenovsky and L. R. A. X. de Menezes. Unscented Transform based Low Complexity Performance Assessment for Adaptive LCMV Filters European Signal Processing Conference (EUSIPCO 2015), submitted on February 27, 2015.
- [2*] R. S. Ferreira Júnior, J. P. C. L. da Costa, R. Zelenovsky and L. R. A. X. de Menezes. Unscented Transform based Low Complex Performance Assessment for Reduced Rank Adaptive LCMV Filters SpringerCircuits, Systems & Signal Processing (CSSP), Submitted on April 17th, 2015, CSSP-D-15-00344.
- [3*] R. S. Ferreira Júnior, M. A. M. Marinho, K. Liu, J. P. C. L. da Costa, A. V. Amaral, and H. C. So, "Improved landing radio altimeter for unmanned aerial vehicles based on an antenna array," in *IEEE IV International Conference on Ultra Modern Telecommunications and Control Systems (ICUMT)*, 2012, best paper award.
- [4*] J. Milanezi Junior, J. P. C. L. da Costa, R. S. Ferreira Junior, M. A. M. Marinho, R. A. Shayani, and R. T. de Sousa Junior, "Energy Harvesting Photovoltaic System to Charge a Cell Phone in Indoor Environments," International Conference on Composite Materials & Renewable Energy Applications 2014, Sousse, Tunisia, Jan 2014.
- [5*] J. Milanezi Junior, J. P. C. L. da Costa, R. S. Ferreira Junior, M. A. M. Marinho, R. A. Shayani, and R. T. de Sousa Junior, SISTEMA FOTOVOLTAICO DE CAPTAÇÃO DE ENERGIA PARA CARGA DE APARELHOS CELULARES EM AMBIENTES FECHADOS, V CONGRESSO BRASILEIRO DE ENERGIA SOLAR, Mar 2014.
- [6*] M. A. M. Marinho, R. S. Ferreira Júnior, J. P. C. L. da Costa, E. P. de Freitas, K. Liu, A. A. H. Cheung, R. T. de Sousa Jr., and R. Zelenovsky, "Antenna array based positioning scheme for unmanned aerial vehicles," in *17th International ITG Workshop on Smart Antennas (WSA 2013)*, 2013.
- [7*] R. S. Ferreira Júnior, M. A. M. Marinho, J. P. C. L. da Costa, A. V. Amaral, and R. T. de Sousa Jr., "Rádio Altimetro baseado em Arranjo de Antenas," Processo N°. : BR 10 2013 002620 4, INPI.
- [8*] J. Milanezi Junior, J. P. C. L. da Costa, R. S. Ferreira Júnior, M. A. M. Marinho, and E. P. de Freitas, "ARRANJO E MÉTODO PARA GERAÇÃO DE ENERGIA ELÉTRICA POR MEIO DE ENGUIAS DISPOSTAS EM AQUÁRIO," Processo N°. : BR 10 2013 011210 0, INPI.

REFERENCES

- [1] L. R. A. X. de Menezes, J. B. J. Pereira, and G. A. Borges, “Statistical model of induced ground voltage using the TLM method,” *IEEE International Symposium on Electromagnetic Compatibility*, 2008.
- [2] L. R. A. X. de Menezes, A. Ajayi, C. Christopoulos, P. Sewell, and G. A. Borges, “Efficient computation of stochastic electromagnetic problems using unscented transforms,” *IET Sci. Meas. Technol.*, Vol. 2, No. 2, March 2008.
- [3] S. Haykin, *Adaptive Filter Theory*, 3rd ed. Prentice Hall, 1995, ISBN: 978-0133227604.
- [4] S. Chen, S. Tan, and L. Hanzo, “Adaptive beamforming for binary phase shift keying communication systems,” *Signal Processing* 87, Elsevier., pp. 68 – 78, 2007.
- [5] R. K. Miranda, J. P. C. L. da Costa, and F. Antreich, “High accuracy and low complexity adaptive generalized sidelobe cancelers for colored noise scenarios.” *Digital Signal Processing*, Elsevier., 2014.
- [6] P. S. Diniz, *Adaptive Filtering - Algorithms and Practical Implementation*, 3rd ed. Springer, May 2008, ISBN: 978-0-387-31274-3.
- [7] R. C. Lamare, L. Wang, and R. Fa, “Adaptive reduced-rank LCMV beamforming algorithms based on joint iterative optimization of filters: Design and analysis,” *Elsevier Signal Processing*, vol. 90 - Issue 2, pp. 640–652, February 2010.
- [8] R. S. Ferreira Júnior, J. P. C. L. da Costa, R. Zelenovsky, and L. R. A. X. de Menezes, “Unscented transform based low complex performance assessment for reduced rank adaptive lcmv filters,” *SpringerCircuits, Systems & Signal Processing (CSSP)*, Submitted on April 17th, 2015, CSSP-D-15-00344, 2015.
- [9] R. S. Ferreira Júnior, J. P. C. L. da Costa, R. Nock, R. Zelenovsky, and L. R. A. X. de Menezes, “Unscented transform based low complexity performance assessment for adaptive lcmv filters,” in *European Signal Processing Conference (EUSIPCO 2015)*, submitted on February 27, 2015, 2015.
- [10] R. S. Ferreira Júnior, M. A. M. Marinho, K. Liu, J. P. C. L. da Costa, A. V. Amaral, and H. C. So, “Improved landing radio altimeter for unmanned aerial vehicles based on an antenna array,” *IEEE IV International Conference on Ultra Modern Telecommunications and Control Systems (ICUMT) 2012, Saint Petersburg, Russia, best paper award*.

- [11] M. Vidmar, "A landing radio altimeter for small aircraft," in *12th International Power Electronics and Motion Control Conference*, 2006.
- [12] J. A. Gubner, *Probability and Random Processes for Electrical and Computer Engineers*, 1st ed. Cambridge University Press, 2006, ISBN: 978-0-521-86470-1.
- [13] A. Papoulis, *Probability, Random Variables, and Stochastic Processes*, 3rd ed., McGraw-Hill, Ed. New York: McGraw-Hill, 1991.
- [14] M. Paul L, *Introductory Probability and Statistical Applications*, ISBN 978-0201047141, 2nd ed., ser. World Student, A. Wesley, Ed. Addison Wesley, 1970.
- [15] H. Anton, *Calculus: A New Horizon*, 6th ed., Wiley, Ed., New York, 1999.
- [16] S. Julier and J. Uhlmann, "A general method for approximating nonlinear transformations of probability distributions," *Eng. Dept., Univ. Oxford, Tech. Rep., Oxford*.
- [17] S. J. Julier and J. K. Uhlmann, "A new extension of the kalman filter to nonlinear systems," in *Int. symp. aerospace/defense sensing, simul. and controls*, vol. 3, no. 26. Orlando, FL, 1997, pp. 3-2.
- [18] A. Papoulis, *The Fourier Integral and its Applications*. McGraw-Hill Book Company Inc., 1962.
- [19] B. D. V. Veen and K. M. Buckley, "Beamforming: A versatile approach to spatial filtering," *IEEE Acoustics, Speech and Signal Processing Magazine (ASSP)*, pp. 4-24, April 1988.
- [20] M. A. M. Marinho, F. Antreich, J. P. C. L. da Costa, and J. A. Nossek, "Reduced Rank TLS Array Interpolation for DOA Estimation," in *18th International ITG Workshop on Smart Antennas (WSA 2014)*, 2014.
- [21] L. R. de Menezes, A. J. Soares, F. C. Silva, M. A. Terada, and D. Correia, "A new procedure for assessing the sensitivity of antennas using the unscented transform," *Antennas and Propagation, IEEE Transactions on*, vol. 58, no. 3, pp. 988-993, 2010.
- [22] L. De Menezes, D. Thomas, C. Christopoulos, A. Ajayi, and P. Sewell, "The use of unscented transforms for statistical analysis in emc," in *Electromagnetic Compatibility-EMC Europe, 2008 International Symposium on*. IEEE, 2008, pp. 1-5.
- [23] L. R. de Menezes, A. Ajayi, C. Christopoulos, P. Sewell, and G. A. Borges, "Efficient computation of stochastic electromagnetic problems using unscented transforms," *IET Science, Measurement & Technology*, vol. 2, no. 2, pp. 88-95, 2008.
- [24] R. A. Horn and C. R. Johnson, *Topics in Matrix Analysis*. Cambridge, England: Cambridge University Press, 1994.
- [25] R. D. Schafer, *An Introduction to Nonassociative Algebras*. New York: Dover., 1996.
- [26] S. Haykin, *Communication Systems*, ISBN 0-471-17869-1, 4th ed., J. W. . Sons, Ed. John Wiley & Sons, 2000.

- [27] B. P. Lathi, *Modern Digital and Analog Communication Systems*, 3rd ed., T. O. S. in Electrical and I. -. Computer Engineering, Eds. Oxford University Press, March 26 1998.
- [28] M. Abramowitz and I. A. Stegun, *Handbook of Mathematical Functions with Formulas, Graphs, and Mathematical Tables*, ninth printing ed., D. Publications, Ed. New York: Dover Publications, 1970.
- [29] G. B. T. Jr. and R. L. Finney, *Calculus and Analytic Geometry*, ISBN 0-201-53174-7, 9th ed., A. Wesley, Ed. Addison Wesley, 1996.
- [30] M. Greenberg, *Advanced Engineering Mathematics*, ISBN 0-13-321431-1, 2nd ed., P. Hall, Ed. Prentice Hall, 1998.
- [31] G. Stimson, *Introduction to Airborne Radar*, Library of Congress: 8383041, 1st ed., H. A. Company, Ed. El Segundo, California: Hughes Aircraft Company, 1983.
- [32] F. N. E., *Radar Design Principles - Signal Processing and the Environment*, Library of Congress: 7980973. McGraw-Hill Book Company, New York,, 1969.
- [33] W. Mansfeld, *Funkortungs- und Funknavigationsanlagen*, ISBN 3-7785-2202-7. Hüthig Buch Verlag GmbH, Heidelberg, 1994.
- [34] L. G. Maloratsky, "An aircraft single-antenna fm radio altimeter," May 2003.
- [35] M. Skolnik, *Radar Handbook: Third Edition*, ISBN: 0071485473. McGraw-Hill, 2001.
- [36] ———, *Radar Handbook: Second Edition*, ISBN: 0071128026. McGraw-Hill, 1991.
- [37] R. E. Best, *Phase-Lock Loops*, ISBN: 0070050503. McGraw-Hill, New York., 1984.